

Bernhard Schweizer · Daixing Lu

Semi-implicit co-simulation approach for solver coupling

Received: 16 September 2013 / Accepted: 6 June 2014 / Published online: 2 August 2014
© Springer-Verlag Berlin Heidelberg 2014

Abstract Co-simulation methods are used to couple two or more subsystem solvers in time domain. Considering mechanical systems, the subsystems can be coupled in two different ways, namely either by applied forces/torques (i.e., by physical force/torque laws) or by constraint forces/torques (i.e., by algebraic constraint equations). Here, we present and analyze a semi-implicit co-simulation method for the case that the subsystems are coupled by applied forces/torques. The semi-implicit approach (predictor/corrector approach) analyzed here is more stable than explicit coupling methods and numerically more efficient than full-implicit coupling schemes. Furthermore, the approach takes only into account partial derivatives of the state variables with respect to the coupling variables so that the Jacobian matrix, which is required for the corrector step, has very small dimensions. For that reason, this semi-implicit approach can be implemented very easily and very time-efficiently, especially for the case that commercial codes without full solver access have to be coupled. Within this paper, we focus on mechanical systems. However, the presented method may also be applied to couple arbitrary non-mechanical systems and arbitrary solvers.

Keywords Co-simulation · Solver coupling · Parallelization · Subcycling · Implicit · Semi-implicit · Coupling by constitutive laws

1 Introduction

Solver coupling is applied in various fields of application [1–8, 14–16, 20, 22]. Applying a co-simulation approach, the overall system is decomposed into two (or more) subsystems. In the paper at hand, we only consider two coupled subsystems. Generally, the subsystems can be coupled by physical force/torque laws (i.e., by applied forces/torques) [11, 12] or by algebraic constraint equations (i.e., by reaction forces/torques) [9, 13, 17–19]. Here, we only consider solver coupling by applied forces/torques.

Concerning the decomposition of the overall system into two subsystems, three basic decomposition techniques may be distinguished in connection with applied -force/torque coupling: the *force/force*-, the *force/displacement*- and the *displacement/displacement-decomposition* approach.

In order to couple the decomposed subsystems, coupling variables (subsystem input and output variables) have to be introduced. For the numerical integration of the decomposed system, a macro-time grid—i.e., macro-time points T_0, T_1, \dots, T_N —has to be defined. Within this paper, an equidistant macro-time grid is used, i.e., the macro-step size $H = T_{N+1} - T_N$ is assumed to be constant. Applying a co-simulation approach (i.e., a weak coupling approach), both subsystems integrate independently between the macro-time points. Only at the

B. Schweizer (✉) · D. Lu
Department of Mechanical Engineering, Institute of Applied Dynamics, Technical University Darmstadt, Petersenstrasse 30,
64287 Darmstadt, Germany
E-mail: schweizer@sds.tu-darmstadt.de

macro-time points, the coupling variables are interchanged between the subsystems. For the subsystem integration from one to the next macro-time point ($T_N \rightarrow T_{N+1}$), the coupling variables have to be approximated (extrapolated/interpolated) by appropriate approximation polynomials (e.g., by Lagrange polynomials).

Co-simulation approaches can be subdivided into explicit, implicit and semi-implicit methods. Explicit methods are simple to implement. The main advantage of explicit methods is that the macro-time step has not to be repeated. Therefore, the subsystem solvers have not to be reinitialized at the previous macro-time point T_N . A further advantage is that Jacobian matrices are not required. The main drawback of explicit schemes is that they suffer from numerical instabilities. Implicit approaches on the other hand are more stable, but the implementation is more involved, because the macro-time steps have to be repeated and the subsystem solvers have to be reinitialized. Moreover, Jacobian matrices of the subsystems may be necessary.

The semi-implicit method analyzed here is based on a predictor/corrector approach. The method shows—on the one hand—an improved stability behavior compared to explicit approaches, and it is—on the other hand—easier to implement than full-implicit methods. The presented approach requires a Jacobian matrix. However, only partial derivatives of the state vectors of the coupling bodies with respect to the coupling variables have to be calculated. Hence, the dimension of the Jacobian matrix is very small so that the Jacobian matrix may be calculated very time-efficiently (practically in parallel with the predictor step). As for full-implicit methods, solver reinitialization is necessary, because each macro-time step has to be repeated once (corrector step).

For the reason of a clear representation, we introduce in Sect. 2 the concept of the semi-implicit approach by means of a simple 2-DOF co-simulation test model. In Sect. 3, the approach is generalized for two arbitrary coupled multibody systems. Numerical tests are shown in Sect. 4. In “Appendix A”, we present analytical formulas for approximating the Jacobian matrix. The zero-stability of the semi-implicit co-simulation approach is briefly discussed in “Appendix B”. Some remarks on alternative and simplified coupling formulations are given in Appendices “C” and “D”.

2 Semi-implicit co-simulation approach for linear test model

To explain the general idea of the semi-implicit coupling approach, we consider the probably most simple co-simulation test model, namely the linear two-mass oscillator (masses m_1/m_2 , spring constants c_1/c_2 , damping coefficients d_1/d_2 , coupling-spring constant c_c , coupling-damper coefficient d_c), see Fig. 1. The two-mass oscillator may be interpreted as two single-mass oscillators, which are coupled by the linear spring c_c and the linear damper d_c . The oscillator has two degrees of freedom described by the coordinates x_1/x_2 and the corresponding velocities v_1/v_2 . The springs are assumed to be stress-free for $x_1 = x_2 = 0$. The equations of motion for the autonomous system read as

$$\begin{aligned} \dot{x}_1 &= v_1, \\ \dot{v}_1 &= -\frac{c_1}{m_1}x_1 - \frac{d_1}{m_1}v_1 + \frac{c_c}{m_1} \cdot (x_2 - x_1) + \frac{d_c}{m_1} \cdot (v_2 - v_1), \\ \dot{x}_2 &= v_2, \\ \dot{v}_2 &= -\frac{c_2}{m_2}x_2 - \frac{d_2}{m_2}v_2 - \frac{c_c}{m_2} \cdot (x_2 - x_1) - \frac{d_c}{m_2} \cdot (v_2 - v_1). \end{aligned} \quad (1)$$

The initial conditions are given by

$$\begin{aligned} x_1(t=0) &= x_{1,0}, & v_1(t=0) &= v_{1,0}, \\ x_2(t=0) &= x_{2,0}, & v_2(t=0) &= v_{2,0}. \end{aligned} \quad (2)$$

The overall system (1) can be decomposed into two subsystems using three different approaches, namely the force/force-, the force/displacement- and the displacement/displacement-coupling approach. These three decomposition techniques are introduced next.

2.1 Force/force-coupling

Applying the force/force-coupling approach, the overall system is decomposed into two subsystems so that both subsystems are force-driven single-mass oscillators, see Fig. 2. The single-mass oscillators are excited

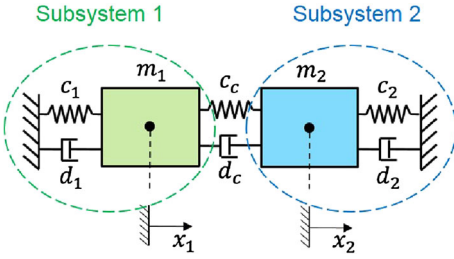


Fig. 1 Linear two-mass oscillator: interpretation as two coupled single-mass oscillators

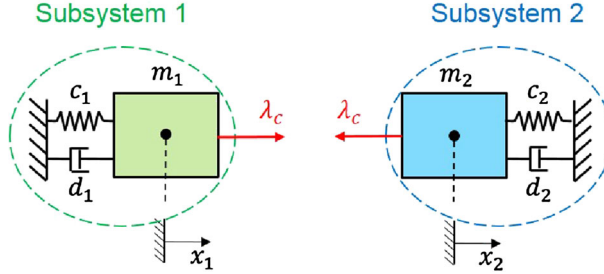


Fig. 2 Linear two-mass oscillator: force/force-coupling approach

by the coupling force λ_c , which can be expressed as a function of the subsystem states. The physical force law for λ_c is implicitly defined by the coupling condition g_c .

The decomposed system is described by the following semi-explicit index-1 DAE system

Subsystem 1:

$$\dot{x}_1 = v_1, \quad \dot{v}_1 = -\frac{c_1}{m_1}x_1 - \frac{d_1}{m_1}v_1 + \frac{\lambda_c}{m_1}, \quad (3a)$$

Subsystem 2:

$$\dot{x}_2 = v_2, \quad \dot{v}_2 = -\frac{c_2}{m_2}x_2 - \frac{d_2}{m_2}v_2 - \frac{\lambda_c}{m_2}, \quad (3b)$$

Coupling condition:

$$g_{\lambda} := \lambda_c - c_c \cdot (x_2 - x_1) - d_c \cdot (v_2 - v_1) = 0. \quad (3c)$$

The semi-implicit co-simulation approach for the decomposed system (3a)–(3c) is accomplished in three steps. To explain the method, we analyze the general macro-time step from T_N to T_{N+1} . For the reason of a clear representation, we consider in Sect. 2 the case that the coupling force λ_c is approximated by constant polynomials. The general case of higher-order approximation is discussed in Sect. 3. At the beginning of the macro-time step, the state variables and the coupling variable are assumed to be known

$$x_1(t = T_N) = x_{1,N}, \quad v_1(t = T_N) = v_{1,N}, \quad (4a)$$

$$x_2(t = T_N) = x_{2,N}, \quad v_2(t = T_N) = v_{2,N}, \quad (4b)$$

$$\lambda_c(t = T_N) = \lambda_{c,N}.$$

Step 1: Predictor step

- Integration of subsystem 1 and subsystem 2 from T_N to T_{N+1} with initial conditions (4a) and with the predicted (extrapolated) coupling force

$$\lambda_c^p(t) = \lambda_{c,N+1}^p = \lambda_{c,N} = \text{const.} \quad (5)$$

yields the predicted state variables at the macro-time point T_{N+1}

$$\begin{aligned} x_{1,N+1}^p &= x_{1,N+1}(\lambda_{c,N+1}^p), & v_{1,N+1}^p &= v_{1,N+1}(\lambda_{c,N+1}^p), \\ x_{2,N+1}^p &= x_{2,N+1}(\lambda_{c,N+1}^p), & v_{2,N+1}^p &= v_{2,N+1}(\lambda_{c,N+1}^p). \end{aligned} \quad (6)$$

Note that for the simple case of constant extrapolation in the time interval $[T_N, T_{N+1}]$, the predicted coupling force $\lambda_c^p(t)$ equals the corrected coupling force $\lambda_{c,N}$ at the previous macro-time point T_N .

Step 2: Calculation of corrected coupling force

- Integration of subsystem 1 and subsystem 2 from T_N to T_{N+1} with initial conditions (4a) and with the perturbed predicted coupling force

$$\lambda_{c,N+1}^{pp\lambda} = \lambda_{c,N+1}^p + \Delta\lambda_c = \text{const.} \quad (7)$$

yields the perturbed predicted state variables at the macro-time point T_{N+1}

$$\begin{aligned} x_{1,N+1}^{pp\lambda} &= x_{1,N+1}(\lambda_{c,N+1}^{pp\lambda}), & v_{1,N+1}^{pp\lambda} &= v_{1,N+1}(\lambda_{c,N+1}^{pp\lambda}), \\ x_{2,N+1}^{pp\lambda} &= x_{2,N+1}(\lambda_{c,N+1}^{pp\lambda}), & v_{2,N+1}^{pp\lambda} &= v_{2,N+1}(\lambda_{c,N+1}^{pp\lambda}). \end{aligned} \quad (8)$$

It should be mentioned that $\Delta\lambda_c$ is a user-defined increment.

- With the predicted and the perturbed predicted state variables, the partial derivatives of the state variables with respect to the coupling force can be approximated by finite differences

$$\begin{aligned} \frac{\partial x_{1,N+1}}{\partial \lambda_{c,N+1}} \Big|_{\lambda_{c,N+1}^p} &= \lim_{\Delta\lambda_c \rightarrow 0} \frac{x_{1,N+1}(\lambda_{c,N+1}^p + \Delta\lambda_c) - x_{1,N+1}(\lambda_{c,N+1}^p)}{\Delta\lambda_c} \approx \frac{x_{1,N+1}^{pp\lambda} - x_{1,N+1}^p}{\Delta\lambda_c}, \\ \frac{\partial v_{1,N+1}}{\partial \lambda_{c,N+1}} \Big|_{\lambda_{c,N+1}^p} &= \lim_{\Delta\lambda_c \rightarrow 0} \frac{v_{1,N+1}(\lambda_{c,N+1}^p + \Delta\lambda_c) - v_{1,N+1}(\lambda_{c,N+1}^p)}{\Delta\lambda_c} \approx \frac{v_{1,N+1}^{pp\lambda} - v_{1,N+1}^p}{\Delta\lambda_c}, \\ \frac{\partial x_{2,N+1}}{\partial \lambda_{c,N+1}} \Big|_{\lambda_{c,N+1}^p} &= \lim_{\Delta\lambda_c \rightarrow 0} \frac{x_{2,N+1}(\lambda_{c,N+1}^p + \Delta\lambda_c) - x_{2,N+1}(\lambda_{c,N+1}^p)}{\Delta\lambda_c} \approx \frac{x_{2,N+1}^{pp\lambda} - x_{2,N+1}^p}{\Delta\lambda_c}, \\ \frac{\partial v_{2,N+1}}{\partial \lambda_{c,N+1}} \Big|_{\lambda_{c,N+1}^p} &= \lim_{\Delta\lambda_c \rightarrow 0} \frac{v_{2,N+1}(\lambda_{c,N+1}^p + \Delta\lambda_c) - v_{2,N+1}(\lambda_{c,N+1}^p)}{\Delta\lambda_c} \approx \frac{v_{2,N+1}^{pp\lambda} - v_{2,N+1}^p}{\Delta\lambda_c}. \end{aligned} \quad (9)$$

- With the help of the partial derivatives, a corrected (i.e., improved) value for the coupling force can be derived for the time interval $[T_N, T_{N+1}]$. At the fixed time point T_{N+1} , $g_{c\lambda,N+1}$ can be considered as a function of the coupling force $\lambda_{c,N+1}$

$$\begin{aligned} g_{c\lambda,N+1}(\lambda_{c,N+1}) &:= \lambda_{c,N+1} - c_c \cdot (x_{2,N+1}(\lambda_{c,N+1}) - x_{1,N+1}(\lambda_{c,N+1})) \\ &\quad - d_c \cdot (v_{2,N+1}(\lambda_{c,N+1}) - v_{1,N+1}(\lambda_{c,N+1})). \end{aligned} \quad (10)$$

Choosing $\lambda_{c,N+1}^p$ as expansion point and neglecting the higher-order terms $\mathcal{O}(\lambda_{c,N+1}^2)$, a Taylor series expansion of $g_{c\lambda,N+1}(\lambda_{c,N+1})$ with respect to $\lambda_{c,N+1}$ yields the linearized coupling condition

$$\begin{aligned} g_{c\lambda,N+1}^{linear}(\lambda_{c,N+1}) &:= g_{c\lambda,N+1}(\lambda_{c,N+1}^p) + \left. \frac{\partial g_{c\lambda,N+1}}{\partial \lambda_{c,N+1}} \right|_{\lambda_{c,N+1}^p} \cdot (\lambda_{c,N+1} - \lambda_{c,N+1}^p) \\ &= \lambda_{c,N+1}^p - c_c \cdot (x_{2,N+1}(\lambda_{c,N+1}^p) - x_{1,N+1}(\lambda_{c,N+1}^p)) - d_c \cdot (v_{2,N+1}(\lambda_{c,N+1}^p) - v_{1,N+1}(\lambda_{c,N+1}^p)) \\ &\quad + \left[1 - c_c \cdot \left(\left. \frac{\partial x_{2,N+1}}{\partial \lambda_{c,N+1}} \right|_{\lambda_{c,N+1}^p} - \left. \frac{\partial x_{1,N+1}}{\partial \lambda_{c,N+1}} \right|_{\lambda_{c,N+1}^p} \right) \right. \\ &\quad \left. - d_c \cdot \left(\left. \frac{\partial v_{2,N+1}}{\partial \lambda_{c,N+1}} \right|_{\lambda_{c,N+1}^p} - \left. \frac{\partial v_{1,N+1}}{\partial \lambda_{c,N+1}} \right|_{\lambda_{c,N+1}^p} \right) \right] \cdot (\lambda_{c,N+1} - \lambda_{c,N+1}^p) = 0. \end{aligned} \quad (11)$$

In general, the predicted state variables and the predicted coupling force do not fulfill the coupling condition, i.e., $g_{c\lambda,N+1}(\lambda_{c,N+1}^p) := \lambda_{c,N+1}^p - c_c \cdot (x_{2,N+1}(\lambda_{c,N+1}^p) - x_{1,N+1}(\lambda_{c,N+1}^p)) - d_c \cdot (v_{2,N+1}(\lambda_{c,N+1}^p) - v_{1,N+1}(\lambda_{c,N+1}^p))$

$-v_{1,N+1}(\lambda_{c,N+1}^p)) \neq 0$. An improved coupling force, which at least fulfills the linearized coupling condition 11, can be derived by solving Eq. 11 for $\lambda_{c,N+1}$. One obtains

$$\begin{aligned} \lambda_{c,N+1} &= \lambda_{c,N+1}^p \\ &- \frac{\lambda_{c,N+1}^p - c_c \cdot (x_{2,N+1}(\lambda_{c,N+1}^p) - x_{1,N+1}(\lambda_{c,N+1}^p)) - d_c \cdot (v_{2,N+1}(\lambda_{c,N+1}^p) - v_{1,N+1}(\lambda_{c,N+1}^p))}{\left[1 - c_c \cdot \left(\frac{\partial x_{2,N+1}}{\partial \lambda_{c,N+1}} \Big|_{\lambda_{c,N+1}^p} - \frac{\partial x_{1,N+1}}{\partial \lambda_{c,N+1}} \Big|_{\lambda_{c,N+1}^p} \right) - d_c \cdot \left(\frac{\partial v_{2,N+1}}{\partial \lambda_{c,N+1}} \Big|_{\lambda_{c,N+1}^p} - \frac{\partial v_{1,N+1}}{\partial \lambda_{c,N+1}} \Big|_{\lambda_{c,N+1}^p} \right) \right]}. \end{aligned} \quad (12)$$

Step 3: Corrector step

- Integration of subsystem 1 and subsystem 2 from T_N to T_{N+1} with initial conditions (4a) and with the corrected coupling force $\lambda_{c,N+1}$ from Eq. (12) yields the corrected states

$$\begin{aligned} x_{1,N+1} &= x_{1,N+1}(\lambda_{c,N+1}), & v_{1,N+1} &= v_{1,N+1}(\lambda_{c,N+1}), \\ x_{2,N+1} &= x_{2,N+1}(\lambda_{c,N+1}), & v_{2,N+1} &= v_{2,N+1}(\lambda_{c,N+1}). \end{aligned} \quad (13)$$

- Remark: The corrected state variables have been calculated based on the linearized coupling condition (11). For the linear co-simulation test model, Eqs. (10) and (11) are equivalent since the states depend only linearly on λ_c so that the corrected coupling force according to Eq. (12) also fulfills the coupling condition (10). For general nonlinear problems, however, the corrected states and the corrected coupling force do not fulfill the nonlinear coupling condition, i.e.,

$$\begin{aligned} g_{c\lambda,N+1}(\lambda_{c,N+1}) &:= \lambda_{c,N+1} - c_c \cdot (x_{2,N+1}(\lambda_{c,N+1}) - x_{1,N+1}(\lambda_{c,N+1})) \\ &- d_c \cdot (v_{2,N+1}(\lambda_{c,N+1}) - v_{1,N+1}(\lambda_{c,N+1})) \neq 0. \end{aligned}$$

To get a consistent corrected coupling force, the coupling force may in a final evaluation step be calculated by the coupling condition and the corrected state variables, i.e., by

$$\begin{aligned} \lambda_{c,N+1}^{\text{final}} &= c_c \cdot (x_{2,N+1}(\lambda_{c,N+1}) - x_{1,N+1}(\lambda_{c,N+1})) \\ &+ d_c \cdot (v_{2,N+1}(\lambda_{c,N+1}) - v_{1,N+1}(\lambda_{c,N+1})). \end{aligned} \quad (14)$$

Choosing in the nonlinear case $\lambda_{c,N+1}^{\text{final}}$ from Eq. (14) instead of $\lambda_{c,N+1}$ from Eq. (12) as corrected coupling force at the macro-time point T_{N+1} may improve the simulation results and the numerical stability of the approach.

2.2 Force/displacement-coupling

Applying the force/displacement-coupling approach, the overall system is decomposed into two subsystems so that subsystem 1 is a force-driven and subsystem 2 a base-point excited single-mass oscillator,¹ see Fig. 3. In contrast to the force/force-coupling approach, the coupling force λ_c is replaced in subsystem 2 by means of the coupling condition (3c) (i.e., by means of the physical force law). Since the state variables x_1 and v_1 are unknown in subsystem 2, they are replaced in the equations of motion by the additional coupling variables \tilde{x}_1 and \tilde{v}_1 . Due to these additional coupling variables, the two additional coupling conditions g_{cx_1} and g_{cv_1} have to be added.

¹ It should be stressed that the overall system may—in an alternative approach—also be decomposed so that subsystem 1 is a base-point excited and subsystem 2 a force-driven single-mass oscillator (displacement/force-coupling approach). Depending on the subsystem and coupling parameters, both approaches may show a different numerical stability behavior.

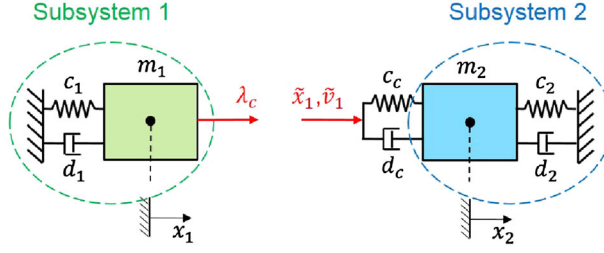


Fig. 3 Linear two-mass oscillator: force/displacement-coupling approach

The decomposed system is described by the following semi-explicit index-1 DAE system

Subsystem 1:

$$\begin{aligned}\dot{x}_1 &= v_1, \\ \dot{v}_1 &= -\frac{c_1}{m_1}x_1 - \frac{d_1}{m_1}v_1 + \frac{\lambda_c}{m_1},\end{aligned}\tag{15a}$$

Subsystem 2:

$$\begin{aligned}\dot{x}_2 &= v_2, \\ \dot{v}_2 &= -\frac{c_2}{m_2}x_2 - \frac{d_2}{m_2}v_2 - \frac{c_c}{m_2} \cdot (x_2 - \tilde{x}_1) - \frac{d_c}{m_2} \cdot (v_2 - \tilde{v}_1),\end{aligned}\tag{15b}$$

Coupling conditions:

$$\begin{aligned}g_{c\lambda} &:= \lambda_c - c_c \cdot (x_2 - x_1) - d_c \cdot (v_2 - v_1) = 0, \\ g_{cx_1} &:= \tilde{x}_1 - x_1 = 0, \\ g_{cv_1} &:= \tilde{v}_1 - v_1 = 0.\end{aligned}\tag{15c}$$

To illustrate the force/displacement-coupling approach, we again consider the general macro-time step from \$T_N\$ to \$T_{N+1}\$. As in Sect. 2.1, we assume that the coupling variables—i.e., \$\lambda_c\$, \$\tilde{x}_1\$ and \$\tilde{v}_1\$—are approximated by constant polynomials. At the beginning of the macro-time step, the state and coupling variables are assumed to be known

$$x_1(t = T_N) = x_{1,N}, \quad v_1(t = T_N) = v_{1,N},\tag{16a}$$

$$x_2(t = T_N) = x_{2,N}, \quad v_2(t = T_N) = v_{2,N},$$

$$\lambda_c(t = T_N) = \lambda_{c,N}, \quad \tilde{x}_1(t = T_N) = \tilde{x}_{1,N}, \quad \tilde{v}_1(t = T_N) = \tilde{v}_{1,N}.\tag{16b}$$

Step 1: Predictor step

- Using the initial conditions (16a) and the predicted (extrapolated) coupling variables

$$\begin{aligned}\lambda_c^p(t) &= \lambda_{c,N+1}^p = \lambda_{c,N} = \text{const.}, \\ \tilde{x}_1^p(t) &= \tilde{x}_{1,N+1}^p = \tilde{x}_{1,N} = \text{const.}, \\ \tilde{v}_1^p(t) &= \tilde{v}_{1,N+1}^p = \tilde{v}_{1,N} = \text{const.},\end{aligned}\tag{17}$$

integration of subsystem 1 and subsystem 2 from \$T_N\$ to \$T_{N+1}\$ yields the predicted state variables at the macro-time point \$T_{N+1}\$

$$\begin{aligned}x_{1,N+1}^p &= x_{1,N+1}(\lambda_{c,N+1}^p), & v_{1,N+1}^p &= v_{1,N+1}(\lambda_{c,N+1}^p), \\ x_{2,N+1}^p &= x_{2,N+1}(\tilde{x}_{1,N+1}^p, \tilde{v}_{1,N+1}^p), & v_{2,N+1}^p &= v_{2,N+1}(\tilde{x}_{1,N+1}^p, \tilde{v}_{1,N+1}^p).\end{aligned}\tag{18}$$

Please note again that using constant extrapolation polynomials in the time interval \$[T_N, T_{N+1}]\$, the predicted coupling variables equal the corrected coupling variables at the previous macro-time point \$T_N\$.

Step 2: Calculation of corrected coupling variables

- By integrating subsystem 1 from T_N to T_{N+1} with the initial conditions (16a) and with the perturbed predicted coupling variable

$$\lambda_{c,N+1}^{pp\lambda} = \lambda_{c,N+1}^p + \Delta\lambda_c = \text{const.}, \quad (19)$$

one obtains the perturbed predicted state variables at the macro-time point T_{N+1}

$$x_{1,N+1}^{pp\lambda} = x_{1,N+1}(\lambda_{c,N+1}^{pp\lambda}), \quad v_{1,N+1}^{pp\lambda} = v_{1,N+1}(\lambda_{c,N+1}^{pp\lambda}). \quad (20)$$

Using the predicted coupling variable $\tilde{v}_{1,N+1}^p$ and the perturbed predicted coupling variable

$$\tilde{x}_{1,N+1}^{pp_x} = \tilde{x}_{1,N+1}^p + \Delta\tilde{x}_1 = \text{const.}, \quad (21)$$

an integration of subsystem 2 from T_N to T_{N+1} with the initial conditions (16a) results in the following perturbed predicted state variables at the macro-time point T_{N+1}

$$x_{2,N+1}^{pp_x} = x_{2,N+1}(\tilde{x}_{1,N+1}^{pp_x}, \tilde{v}_{1,N+1}^p), \quad v_{2,N+1}^{pp_x} = v_{2,N+1}(\tilde{x}_{1,N+1}^{pp_x}, \tilde{v}_{1,N+1}^p). \quad (22)$$

A corresponding integration with the predicted coupling variable $\tilde{x}_{1,N+1}^p$ and the perturbed predicted coupling variable

$$\tilde{v}_{1,N+1}^{pp_v} = \tilde{v}_{1,N+1}^p + \Delta\tilde{v}_1 = \text{const.}, \quad (23)$$

yields the perturbed predicted state variables

$$x_{2,N+1}^{pp_v} = x_{2,N+1}(\tilde{x}_{1,N+1}^p, \tilde{v}_{1,N+1}^{pp_v}), \quad v_{2,N+1}^{pp_v} = v_{2,N+1}(\tilde{x}_{1,N+1}^p, \tilde{v}_{1,N+1}^{pp_v}). \quad (24)$$

The increments $\Delta\lambda_c$, $\Delta\tilde{x}_1$ and $\Delta\tilde{v}_1$ have to be specified by the user.

- The partial derivatives of the state variables with respect to the coupling variables can approximately be calculated by finite differences using the predicted and the perturbed predicted state variables

$$\begin{aligned} \frac{\partial x_{1,N+1}}{\partial \lambda_{c,N+1}} \Big|_{\lambda_{c,N+1}^p} &\approx \frac{x_{1,N+1}^{pp\lambda} - x_{1,N+1}^p}{\Delta\lambda_c}, & \frac{\partial v_{1,N+1}}{\partial \lambda_{c,N+1}} \Big|_{\lambda_{c,N+1}^p} &\approx \frac{v_{1,N+1}^{pp\lambda} - v_{1,N+1}^p}{\Delta\lambda_c}, \\ \frac{\partial x_{2,N+1}}{\partial \tilde{x}_{1,N+1}} \Big|_{\tilde{x}_{1,N+1}^p, \tilde{v}_{1,N+1}^p} &\approx \frac{x_{2,N+1}^{pp_x} - x_{2,N+1}^p}{\Delta\tilde{x}_1}, & \frac{\partial v_{2,N+1}}{\partial \tilde{x}_{1,N+1}} \Big|_{\tilde{x}_{1,N+1}^p, \tilde{v}_{1,N+1}^p} &\approx \frac{v_{2,N+1}^{pp_x} - v_{2,N+1}^p}{\Delta\tilde{x}_1}, \\ \frac{\partial x_{2,N+1}}{\partial \tilde{v}_{1,N+1}} \Big|_{\tilde{x}_{1,N+1}^p, \tilde{v}_{1,N+1}^p} &\approx \frac{x_{2,N+1}^{pp_v} - x_{2,N+1}^p}{\Delta\tilde{v}_1}, & \frac{\partial v_{2,N+1}}{\partial \tilde{v}_{1,N+1}} \Big|_{\tilde{x}_{1,N+1}^p, \tilde{v}_{1,N+1}^p} &\approx \frac{v_{2,N+1}^{pp_v} - v_{2,N+1}^p}{\Delta\tilde{v}_1}. \end{aligned} \quad (25)$$

- Corrected (i.e., improved) values for the coupling variables at the time point T_{N+1} can be obtained with the help of the partial derivatives. Regarding the fixed macro-time point T_{N+1} , $g_{c\lambda,N+1}$, $g_{cx_1,N+1}$ and $g_{cv_1,N+1}$ can be considered as functions of $\lambda_{c,N+1}$, $\tilde{x}_{1,N+1}$ and $\tilde{v}_{1,N+1}$

$$\begin{aligned} g_{c\lambda,N+1}(\lambda_{c,N+1}, \tilde{x}_{1,N+1}, \tilde{v}_{1,N+1}) &:= \lambda_{c,N+1} \\ &- c_c \cdot (x_{2,N+1}(\tilde{x}_{1,N+1}, \tilde{v}_{1,N+1}) - x_{1,N+1}(\lambda_{c,N+1})) \\ &- d_c \cdot (v_{2,N+1}(\tilde{x}_{1,N+1}, \tilde{v}_{1,N+1}) - v_{1,N+1}(\lambda_{c,N+1})), \\ g_{cx_1,N+1}(\lambda_{c,N+1}, \tilde{x}_{1,N+1}) &:= \tilde{x}_{1,N+1} - x_{1,N+1}(\lambda_{c,N+1}), \\ g_{cv_1,N+1}(\lambda_{c,N+1}, \tilde{v}_{1,N+1}) &:= \tilde{v}_{1,N+1} - v_{1,N+1}(\lambda_{c,N+1}). \end{aligned} \quad (26)$$

By choosing $e^p = (\lambda_{c,N+1}^p \ \tilde{x}_{1,N+1}^p \ \tilde{v}_{1,N+1}^p)^T$ as expansion point and by neglecting the higher-order terms $\mathcal{O}(\lambda_{c,N+1}^2)$, $\mathcal{O}(\tilde{x}_{1,N+1}^2)$ and $\mathcal{O}(\tilde{v}_{1,N+1}^2)$, linearized coupling conditions can be derived by a Taylor series

expansion of the functions $g_{c\lambda,N+1}$, $g_{cx_1,N+1}$ and $g_{cv_1,N+1}$ with respect to $\lambda_{c,N+1}$, $\tilde{x}_{1,N+1}$ and $\tilde{v}_{1,N+1}$

$$\begin{aligned} g_{c\lambda,N+1}^{\text{linear}}(\lambda_{c,N+1}, \tilde{x}_{1,N+1}, \tilde{v}_{1,N+1}) &:= g_{c\lambda,N+1}(\boldsymbol{e}^p) + \frac{\partial g_{c\lambda,N+1}}{\partial \lambda_{c,N+1}} \Big|_{\boldsymbol{e}^p} \cdot (\lambda_{c,N+1} - \lambda_{c,N+1}^p) \\ &\quad + \frac{\partial g_{c\lambda,N+1}}{\partial \tilde{x}_{1,N+1}} \Big|_{\boldsymbol{e}^p} \cdot (\tilde{x}_{1,N+1} - \tilde{x}_{1,N+1}^p) + \frac{\partial g_{c\lambda,N+1}}{\partial \tilde{v}_{1,N+1}} \Big|_{\boldsymbol{e}^p} \cdot (\tilde{v}_{1,N+1} - \tilde{v}_{1,N+1}^p) \\ &= \lambda_{c,N+1}^p - c_c \cdot (x_{2,N+1}^p - x_{1,N+1}^p) - d_c \cdot (v_{2,N+1}^p - v_{1,N+1}^p) \\ &\quad + \left[1 + c_c \cdot \frac{\partial x_{1,N+1}}{\partial \lambda_{c,N+1}} \Big|_{\boldsymbol{e}^p} + d_c \cdot \frac{\partial v_{1,N+1}}{\partial \lambda_{c,N+1}} \Big|_{\boldsymbol{e}^p} \right] \cdot (\lambda_{c,N+1} - \lambda_{c,N+1}^p) \\ &\quad + \left[-c_c \cdot \frac{\partial x_{2,N+1}}{\partial \tilde{x}_{1,N+1}} \Big|_{\boldsymbol{e}^p} - d_c \cdot \frac{\partial v_{2,N+1}}{\partial \tilde{x}_{1,N+1}} \Big|_{\boldsymbol{e}^p} \right] \cdot (\tilde{x}_{1,N+1} - \tilde{x}_{1,N+1}^p) \\ &\quad + \left[-c_c \cdot \frac{\partial x_{2,N+1}}{\partial \tilde{v}_{1,N+1}} \Big|_{\boldsymbol{e}^p} - d_c \cdot \frac{\partial v_{2,N+1}}{\partial \tilde{v}_{1,N+1}} \Big|_{\boldsymbol{e}^p} \right] \cdot (\tilde{v}_{1,N+1} - \tilde{v}_{1,N+1}^p) = 0, \end{aligned} \quad (27)$$

$$\begin{aligned} g_{cx_1,N+1}^{\text{linear}}(\lambda_{c,N+1}, \tilde{x}_{1,N+1}) &:= g_{cx_1,N+1}(\boldsymbol{e}^p) + \frac{\partial g_{cx_1,N+1}}{\partial \lambda_{c,N+1}} \Big|_{\boldsymbol{e}^p} \cdot (\lambda_{c,N+1} - \lambda_{c,N+1}^p) \\ &\quad + \frac{\partial g_{cx_1,N+1}}{\partial \tilde{x}_{1,N+1}} \Big|_{\boldsymbol{e}^p} \cdot (\tilde{x}_{1,N+1} - \tilde{x}_{1,N+1}^p) \\ &= \tilde{x}_{1,N+1}^p - x_{1,N+1}^p - \frac{\partial x_{1,N+1}}{\partial \lambda_{c,N+1}} \Big|_{\boldsymbol{e}^p} \cdot (\lambda_{c,N+1} - \lambda_{c,N+1}^p) + 1 \cdot (\tilde{x}_{1,N+1} - \tilde{x}_{1,N+1}^p) = 0, \end{aligned} \quad (28)$$

$$\begin{aligned} g_{cv_1,N+1}^{\text{linear}}(\lambda_{c,N+1}, \tilde{v}_{1,N+1}) &:= g_{cv_1,N+1}(\boldsymbol{e}^p) + \frac{\partial g_{cv_1,N+1}}{\partial \lambda_{c,N+1}} \Big|_{\boldsymbol{e}^p} \cdot (\lambda_{c,N+1} - \lambda_{c,N+1}^p) \\ &\quad + \frac{\partial g_{cv_1,N+1}}{\partial \tilde{v}_{1,N+1}} \Big|_{\boldsymbol{e}^p} \cdot (\tilde{v}_{1,N+1} - \tilde{v}_{1,N+1}^p) \\ &= \tilde{v}_{1,N+1}^p - v_{1,N+1}^p - \frac{\partial v_{1,N+1}}{\partial \lambda_{c,N+1}} \Big|_{\boldsymbol{e}^p} \cdot (\lambda_{c,N+1} - \lambda_{c,N+1}^p) + 1 \cdot (\tilde{v}_{1,N+1} - \tilde{v}_{1,N+1}^p) = 0. \end{aligned} \quad (29)$$

- The predicted state and the predicted coupling variables do not fulfill the coupling conditions in general, i.e., $g_{c\lambda,N+1}(\boldsymbol{e}^p) \neq 0$, $g_{cx_1,N+1}(\boldsymbol{e}^p) \neq 0$ and $g_{cv_1,N+1}(\boldsymbol{e}^p) \neq 0$. Solving Eqs. (27)–(29) for the coupling variables, one gets improved coupling variables, which fulfill the linearized coupling conditions

$$\begin{aligned} g_{c\lambda,N+1}^{\text{linear}}(\lambda_{c,N+1}, \tilde{x}_{1,N+1}, \tilde{v}_{1,N+1}) &= 0 \\ g_{cx_1,N+1}^{\text{linear}}(\lambda_{c,N+1}, \tilde{x}_{1,N+1}) &= 0 \quad \Rightarrow \quad \lambda_{c,N+1}, \tilde{x}_{1,N+1}, \tilde{v}_{1,N+1} \\ g_{cv_1,N+1}^{\text{linear}}(\lambda_{c,N+1}, \tilde{v}_{1,N+1}) &= 0 \end{aligned} \quad (30)$$

Step 3: Corrector step

- Using the corrected coupling variables $\lambda_{c,N+1}$, $\tilde{x}_{1,N+1}$ and $\tilde{v}_{1,N+1}$ from Eq. (30) and integrating subsystem 1 and subsystem 2 from T_N to T_{N+1} with the initial conditions (16a), one obtains the corrected states

$$\begin{aligned} x_{1,N+1} &= x_{1,N+1}(\lambda_{c,N+1}), & v_{1,N+1} &= v_{1,N+1}(\lambda_{c,N+1}), \\ x_{2,N+1} &= x_{2,N+1}(\tilde{x}_{1,N+1}, \tilde{v}_{1,N+1}), & v_{2,N+1} &= v_{2,N+1}(\tilde{x}_{1,N+1}, \tilde{v}_{1,N+1}). \end{aligned} \quad (31)$$

- Remark: For nonlinear problems, the corrected states and the corrected coupling variables do in general not fulfill the nonlinear coupling conditions, i.e., $g_{c\lambda,N+1}(\lambda_{c,N+1}, \tilde{x}_{1,N+1}, \tilde{v}_{1,N+1}) \neq 0$, $g_{cx_1,N+1}(\lambda_{c,N+1}, \tilde{x}_{1,N+1}) \neq 0$ and $g_{cv_1,N+1}(\lambda_{c,N+1}, \tilde{v}_{1,N+1}) \neq 0$, since the corrected state variables have been calculated with the linearized coupling conditions (27)–(29). Consistent corrected coupling variables can be calculated

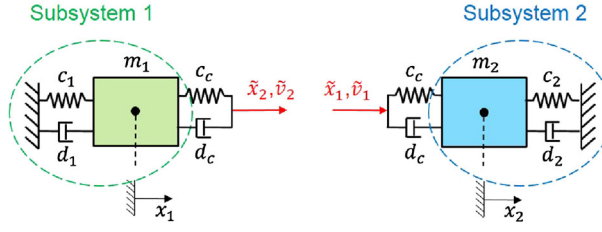


Fig. 4 Linear two-mass oscillator: displacement/displacement-coupling approach

in a final evaluation step with the help of the coupling equations and the corrected state variables by solving

$$\begin{aligned} g_{c\lambda,N+1}(\lambda_{c,N+1}^{\text{final}}, x_{1,N+1}(\lambda_{c,N+1}), v_{1,N+1}(\lambda_{c,N+1}), \\ x_{2,N+1}(\tilde{x}_{1,N+1}, \tilde{v}_{1,N+1}), v_{2,N+1}(\tilde{x}_{1,N+1}, \tilde{v}_{1,N+1})) = 0, \\ g_{cx_{1,N+1}}(\tilde{x}_{1,N+1}^{\text{final}}, x_{1,N+1}(\lambda_{c,N+1})) = 0, \\ g_{cv_{1,N+1}}(\tilde{v}_{1,N+1}^{\text{final}}, v_{1,N+1}(\lambda_{c,N+1})) = 0 \end{aligned} \quad (32)$$

for $\lambda_{c,N+1}^{\text{final}}$, $\tilde{x}_{1,N+1}^{\text{final}}$, $\tilde{v}_{1,N+1}^{\text{final}}$. By choosing $\lambda_{c,N+1}^{\text{final}}$, $\tilde{x}_{1,N+1}^{\text{final}}$, $\tilde{v}_{1,N+1}^{\text{final}}$ from Eq. (32) instead of $\lambda_{c,N+1}$, $\tilde{x}_{1,N+1}$, $\tilde{v}_{1,N+1}$ from Eq. (30) as corrected coupling variables at the macro-time point T_{N+1} may improve the co-simulation results.

2.3 Displacement/displacement-coupling

Applying the displacement/displacement-coupling approach, the overall system is decomposed into two subsystems so that both subsystems are base-point excited single-mass oscillators, see Fig. 4. Therefore, the coupling spring/damper system is duplicated. The coupling variable λ_c is replaced in both subsystems by means of the coupling condition (3c). As a consequence, additional coupling variables have to be defined and additional coupling conditions have to be formulated. The decomposed system is mathematically defined by the following semi-explicit index-1 DAE system

Subsystem 1:

$$\begin{aligned} \dot{x}_1 &= v_1, \\ \dot{v}_1 &= -\frac{c_1}{m_1}x_1 - \frac{d_1}{m_1}v_1 + \frac{c_c}{m_1} \cdot (\tilde{x}_2 - x_1) + \frac{d_c}{m_1} \cdot (\tilde{v}_2 - v_1), \end{aligned} \quad (33a)$$

Subsystem 2:

$$\begin{aligned} \dot{x}_2 &= v_2, \\ \dot{v}_2 &= -\frac{c_2}{m_2}x_2 - \frac{d_2}{m_2}v_2 - \frac{c_c}{m_2} \cdot (x_2 - \tilde{x}_1) - \frac{d_c}{m_2} \cdot (v_2 - \tilde{v}_1), \end{aligned} \quad (33b)$$

Coupling conditions:

$$\begin{aligned} g_{cx_1} &:= \tilde{x}_1 - x_1 = 0, \\ g_{cv_1} &:= \tilde{v}_1 - v_1 = 0, \\ g_{cx_2} &:= \tilde{x}_2 - x_2 = 0, \\ g_{cv_2} &:= \tilde{v}_2 - v_2 = 0. \end{aligned} \quad (33c)$$

To describe the displacement/displacement-coupling approach, we regard the general macro-time step from T_N to T_{N+1} and assume again that the coupling variables—i.e., \tilde{x}_1 , \tilde{v}_1 , \tilde{x}_2 and \tilde{v}_2 —are approximated by constant polynomials. At the beginning of the macro-time step, the state and the coupling variables are assumed to be known

$$x_1(t = T_N) = x_{1,N}, \quad v_1(t = T_N) = v_{1,N}, \quad (34a)$$

$$x_2(t = T_N) = x_{2,N}, \quad v_2(t = T_N) = v_{2,N},$$

$$\tilde{x}_1(t = T_N) = \tilde{x}_{1,N}, \quad \tilde{v}_1(t = T_N) = \tilde{v}_{1,N}, \quad (34b)$$

$$\tilde{x}_2(t = T_N) = \tilde{x}_{2,N}, \quad \tilde{v}_2(t = T_N) = \tilde{v}_{2,N}.$$

Step 1: Predictor step

- By integrating subsystem 1 and subsystem 2 from T_N to T_{N+1} with the initial conditions (34a) and with the predicted (extrapolated) coupling variables

$$\begin{aligned}\tilde{x}_1^p(t) &= \tilde{x}_{1,N+1}^p = \tilde{x}_{1,N} = \text{const.}, & \tilde{v}_1^p(t) &= \tilde{v}_{1,N+1}^p = \tilde{v}_{1,N} = \text{const.}, \\ \tilde{x}_2^p(t) &= \tilde{x}_{2,N+1}^p = \tilde{x}_{2,N} = \text{const.}, & \tilde{v}_2^p(t) &= \tilde{v}_{2,N+1}^p = \tilde{v}_{2,N} = \text{const.},\end{aligned}\quad (35)$$

one gets predicted state variables at the macro-time point T_{N+1}

$$\begin{aligned}x_{1,N+1}^p &= x_{1,N+1}(\tilde{x}_{2,N+1}^p, \tilde{v}_{2,N+1}^p), & v_{1,N+1}^p &= v_{1,N+1}(\tilde{x}_{2,N+1}^p, \tilde{v}_{2,N+1}^p), \\ x_{2,N+1}^p &= x_{2,N+1}(\tilde{x}_{1,N+1}^p, \tilde{v}_{1,N+1}^p), & v_{2,N+1}^p &= v_{2,N+1}(\tilde{x}_{1,N+1}^p, \tilde{v}_{1,N+1}^p).\end{aligned}\quad (36)$$

Step 2: Calculation of corrected coupling variables

- Using the predicted coupling variable $\tilde{v}_{2,N+1}^p$ and the perturbed predicted coupling variable

$$\tilde{x}_{2,N+1}^{pp_x} = \tilde{x}_{2,N+1}^p + \Delta\tilde{x}_2 = \text{const.}, \quad (37)$$

an integration of subsystem 1 from T_N to T_{N+1} with initial conditions (34a) yields the subsequent perturbed predicted state variables at the macro-time point T_{N+1}

$$x_{1,N+1}^{pp_x} = x_{1,N+1}(\tilde{x}_{2,N+1}^{pp_x}, \tilde{v}_{2,N+1}^p), \quad v_{1,N+1}^{pp_x} = v_{1,N+1}(\tilde{x}_{2,N+1}^{pp_x}, \tilde{v}_{2,N+1}^p). \quad (38)$$

Similarly, by using the predicted coupling variable $\tilde{x}_{2,N+1}^p$ and the perturbed predicted coupling variable

$$\tilde{v}_{2,N+1}^{pp_v} = \tilde{v}_{2,N+1}^p + \Delta\tilde{v}_2 = \text{const.}, \quad (39)$$

one obtains the perturbed predicted state variables

$$x_{1,N+1}^{pp_v} = x_{1,N+1}(\tilde{x}_{2,N+1}^p, \tilde{v}_{2,N+1}^{pp_v}), \quad v_{1,N+1}^{pp_v} = v_{1,N+1}(\tilde{x}_{2,N+1}^p, \tilde{v}_{2,N+1}^{pp_v}). \quad (40)$$

Using the perturbed predicted coupling variables $\tilde{x}_{1,N+1}^{pp_x} = \tilde{x}_{1,N+1}^p + \Delta\tilde{x}_1 = \text{const.}$ and $\tilde{v}_{1,N+1}^{pp_v} = \tilde{v}_{1,N+1}^p + \Delta\tilde{v}_1 = \text{const.}$, two equivalent integrations with subsystem 2 yield the perturbed predicted state variables

$$x_{2,N+1}^{pp_x} = x_{2,N+1}(\tilde{x}_{1,N+1}^{pp_x}, \tilde{v}_{1,N+1}^p), \quad v_{2,N+1}^{pp_x} = v_{2,N+1}(\tilde{x}_{1,N+1}^{pp_x}, \tilde{v}_{1,N+1}^p) \quad (41)$$

and

$$x_{2,N+1}^{pp_v} = x_{2,N+1}(\tilde{x}_{1,N+1}^p, \tilde{v}_{1,N+1}^{pp_v}), \quad v_{2,N+1}^{pp_v} = v_{2,N+1}(\tilde{x}_{1,N+1}^p, \tilde{v}_{1,N+1}^{pp_v}). \quad (42)$$

The increments $\Delta\tilde{x}_1$, $\Delta\tilde{v}_1$, $\Delta\tilde{x}_2$ and $\Delta\tilde{v}_2$ are user-defined values, which have to be chosen properly.

- Using the predicted and the perturbed predicted state variables, the partial derivatives of the state variables with respect to the coupling variables can be approximated by finite differences, see Sects. 2.1 and 2.2.
- By making use of the partial derivatives, corrected values for the coupling variables at the time point T_{N+1} can be calculated. Considering the fixed macro-time point T_{N+1} , $g_{cx_1,N+1}$, $g_{cv_1,N+1}$, $g_{cx_2,N+1}$ and $g_{cv_2,N+1}$ can be regarded as functions of $\tilde{x}_{1,N+1}$, $\tilde{v}_{1,N+1}$, $\tilde{x}_{2,N+1}$ and $\tilde{v}_{2,N+1}$

$$\begin{aligned}g_{cx_1,N+1}(\tilde{x}_{1,N+1}, \tilde{x}_{2,N+1}, \tilde{v}_{2,N+1}) &:= \tilde{x}_{1,N+1} - x_1(\tilde{x}_{2,N+1}, \tilde{v}_{2,N+1}), \\ g_{cv_1,N+1}(\tilde{v}_{1,N+1}, \tilde{x}_{2,N+1}, \tilde{v}_{2,N+1}) &:= \tilde{v}_{1,N+1} - v_1(\tilde{x}_{2,N+1}, \tilde{v}_{2,N+1}), \\ g_{cx_2,N+1}(\tilde{x}_{1,N+1}, \tilde{v}_{1,N+1}, \tilde{x}_{2,N+1}) &:= \tilde{x}_{2,N+1} - x_2(\tilde{x}_{1,N+1}, \tilde{v}_{1,N+1}), \\ g_{cv_2,N+1}(\tilde{x}_{1,N+1}, \tilde{v}_{1,N+1}, \tilde{v}_{2,N+1}) &:= \tilde{v}_{2,N+1} - v_2(\tilde{x}_{1,N+1}, \tilde{v}_{1,N+1}).\end{aligned}\quad (43)$$

If we choose $e^p = (\tilde{x}_{1,N+1}^p \ \tilde{v}_{1,N+1}^p \ \tilde{x}_{2,N+1}^p \ \tilde{v}_{2,N+1}^p)^T$ as expansion point and if we neglect the higher-order terms $\mathcal{O}(\tilde{x}_{1,N+1}^2)$, $\mathcal{O}(\tilde{v}_{1,N+1}^2)$, $\mathcal{O}(\tilde{x}_{2,N+1}^2)$ and $\mathcal{O}(\tilde{v}_{2,N+1}^2)$, a Taylor series expansion of $g_{cx_1,N+1}$, $g_{cv_1,N+1}$,

$g_{cx_2,N+1}$ and $g_{cv_2,N+1}$ with respect to $\tilde{x}_{1,N+1}$, $\tilde{v}_{1,N+1}$, $\tilde{x}_{2,N+1}$ and $\tilde{v}_{2,N+1}$ yields the linearized coupling conditions

$$\begin{aligned} g_{cx_1,N+1}^{\text{linear}}(\tilde{x}_{1,N+1}, \tilde{x}_{2,N+1}, \tilde{v}_{2,N+1}) &:= g_{cx_1,N+1}(\boldsymbol{e}^p) + \frac{\partial g_{cx_1,N+1}}{\partial \tilde{x}_{1,N+1}} \Big|_{\boldsymbol{e}^p} \cdot (\tilde{x}_{1,N+1} - \tilde{x}_{1,N+1}^p) \\ &\quad + \frac{\partial g_{cx_1,N+1}}{\partial \tilde{x}_{2,N+1}} \Big|_{\boldsymbol{e}^p} \cdot (\tilde{x}_{2,N+1} - \tilde{x}_{2,N+1}^p) + \frac{\partial g_{cx_1,N+1}}{\partial \tilde{v}_{2,N+1}} \Big|_{\boldsymbol{e}^p} \cdot (\tilde{v}_{2,N+1} - \tilde{v}_{2,N+1}^p) \\ &= \tilde{x}_{1,N+1}^p - x_{1,N+1}^p + 1 \cdot (\tilde{x}_{1,N+1} - \tilde{x}_{1,N+1}^p) - \frac{\partial x_{1,N+1}}{\partial \tilde{x}_{2,N+1}} \Big|_{\boldsymbol{e}^p} \cdot (\tilde{x}_{2,N+1} - \tilde{x}_{2,N+1}^p) \end{aligned} \quad (44)$$

$$\begin{aligned} &\quad - \frac{\partial x_{1,N+1}}{\partial \tilde{v}_{2,N+1}} \Big|_{\boldsymbol{e}^p} \cdot (\tilde{v}_{2,N+1} - \tilde{v}_{2,N+1}^p) = 0, \\ g_{cv_1,N+1}^{\text{linear}}(\tilde{v}_{1,N+1}, \tilde{x}_{2,N+1}, \tilde{v}_{2,N+1}) &:= g_{cv_1,N+1}(\boldsymbol{e}^p) + \frac{\partial g_{cv_1,N+1}}{\partial \tilde{v}_{1,N+1}} \Big|_{\boldsymbol{e}^p} \cdot (\tilde{v}_{1,N+1} - \tilde{v}_{1,N+1}^p) \\ &\quad + \frac{\partial g_{cv_1,N+1}}{\partial \tilde{x}_{2,N+1}} \Big|_{\boldsymbol{e}^p} \cdot (\tilde{x}_{2,N+1} - \tilde{x}_{2,N+1}^p) + \frac{\partial g_{cv_1,N+1}}{\partial \tilde{v}_{2,N+1}} \Big|_{\boldsymbol{e}^p} \cdot (\tilde{v}_{2,N+1} - \tilde{v}_{2,N+1}^p) \\ &= \tilde{v}_{1,N+1}^p - v_{1,N+1}^p + 1 \cdot (\tilde{v}_{1,N+1} - \tilde{v}_{1,N+1}^p) - \frac{\partial v_{1,N+1}}{\partial \tilde{x}_{2,N+1}} \Big|_{\boldsymbol{e}^p} \cdot (\tilde{x}_{2,N+1} - \tilde{x}_{2,N+1}^p) \\ &\quad - \frac{\partial v_{1,N+1}}{\partial \tilde{v}_{2,N+1}} \Big|_{\boldsymbol{e}^p} \cdot (\tilde{v}_{2,N+1} - \tilde{v}_{2,N+1}^p) = 0, \end{aligned} \quad (45)$$

$$\begin{aligned} g_{cx_2,N+1}^{\text{linear}}(\tilde{x}_{1,N+1}, \tilde{v}_{1,N+1}, \tilde{x}_{2,N+1}) &:= g_{cx_2,N+1}(\boldsymbol{e}^p) + \frac{\partial g_{cx_2,N+1}}{\partial \tilde{x}_{1,N+1}} \Big|_{\boldsymbol{e}^p} \cdot (\tilde{x}_{1,N+1} - \tilde{x}_{1,N+1}^p) \\ &\quad + \frac{\partial g_{cx_2,N+1}}{\partial \tilde{v}_{1,N+1}} \Big|_{\boldsymbol{e}^p} \cdot (\tilde{v}_{1,N+1} - \tilde{v}_{1,N+1}^p) + \frac{\partial g_{cx_2,N+1}}{\partial \tilde{x}_{2,N+1}} \Big|_{\boldsymbol{e}^p} \cdot (\tilde{x}_{2,N+1} - \tilde{x}_{2,N+1}^p) \\ &= \tilde{x}_{2,N+1}^p - x_{2,N+1}^p - \frac{\partial x_{2,N+1}}{\partial \tilde{x}_{1,N+1}} \Big|_{\boldsymbol{e}^p} \cdot (\tilde{x}_{1,N+1} - \tilde{x}_{1,N+1}^p) - \frac{\partial x_{2,N+1}}{\partial \tilde{v}_{1,N+1}} \Big|_{\boldsymbol{e}^p} \cdot (\tilde{v}_{1,N+1} - \tilde{v}_{1,N+1}^p) \\ &\quad + 1 \cdot (\tilde{x}_{2,N+1} - \tilde{x}_{2,N+1}^p) = 0, \end{aligned} \quad (46)$$

$$\begin{aligned} g_{cv_2,N+1}^{\text{linear}}(\tilde{x}_{1,N+1}, \tilde{v}_{1,N+1}, \tilde{v}_{2,N+1}) &:= g_{cv_2,N+1}(\boldsymbol{e}^p) + \frac{\partial g_{cv_2,N+1}}{\partial \tilde{x}_{1,N+1}} \Big|_{\boldsymbol{e}^p} \cdot (\tilde{x}_{1,N+1} - \tilde{x}_{1,N+1}^p) \\ &\quad + \frac{\partial g_{cv_2,N+1}}{\partial \tilde{v}_{1,N+1}} \Big|_{\boldsymbol{e}^p} \cdot (\tilde{v}_{1,N+1} - \tilde{v}_{1,N+1}^p) + \frac{\partial g_{cv_2,N+1}}{\partial \tilde{v}_{2,N+1}} \Big|_{\boldsymbol{e}^p} \cdot (\tilde{v}_{2,N+1} - \tilde{v}_{2,N+1}^p) \\ &= \tilde{v}_{2,N+1}^p - v_{2,N+1}^p - \frac{\partial v_{2,N+1}}{\partial \tilde{x}_{1,N+1}} \Big|_{\boldsymbol{e}^p} \cdot (\tilde{x}_{1,N+1} - \tilde{x}_{1,N+1}^p) - \frac{\partial v_{2,N+1}}{\partial \tilde{v}_{1,N+1}} \Big|_{\boldsymbol{e}^p} \cdot (\tilde{v}_{1,N+1} - \tilde{v}_{1,N+1}^p) \\ &\quad + 1 \cdot (\tilde{v}_{2,N+1} - \tilde{v}_{2,N+1}^p) = 0. \end{aligned} \quad (47)$$

- Generally, the predicted state and the predicted coupling variables do not fulfill the coupling conditions, i.e., $g_{cx_1,N+1}(\boldsymbol{e}^p) \neq 0$, $g_{cv_1,N+1}(\boldsymbol{e}^p) \neq 0$, $g_{cx_2,N+1}(\boldsymbol{e}^p) \neq 0$ and $g_{cv_2,N+1}(\boldsymbol{e}^p) \neq 0$. Solving Eqs. (44)–(47) for the coupling variables, corrected (improved) coupling variables can be determined

$$\begin{aligned} g_{cx_1,N+1}^{\text{linear}}(\tilde{x}_{1,N+1}, \tilde{x}_{2,N+1}, \tilde{v}_{2,N+1}) &= 0 \\ g_{cv_1,N+1}^{\text{linear}}(\tilde{v}_{1,N+1}, \tilde{x}_{2,N+1}, \tilde{v}_{2,N+1}) &= 0 \\ g_{cx_2,N+1}^{\text{linear}}(\tilde{x}_{1,N+1}, \tilde{v}_{1,N+1}, \tilde{x}_{2,N+1}) &= 0 \quad \Rightarrow \quad \tilde{x}_{1,N+1}, \tilde{v}_{1,N+1}, \tilde{x}_{2,N+1}, \tilde{v}_{2,N+1} \\ g_{cv_2,N+1}^{\text{linear}}(\tilde{x}_{1,N+1}, \tilde{v}_{1,N+1}, \tilde{v}_{2,N+1}) &= 0 \end{aligned} \quad (48)$$

Step 3: Corrector step

- Making use of the corrected coupling variables $\tilde{x}_{1,N+1}$, $\tilde{v}_{1,N+1}$, $\tilde{x}_{2,N+1}$ and $\tilde{v}_{2,N+1}$ from Eq. (48), an integration of subsystem 1 and subsystem 2 from T_N to T_{N+1} with initial conditions (34a) provides the

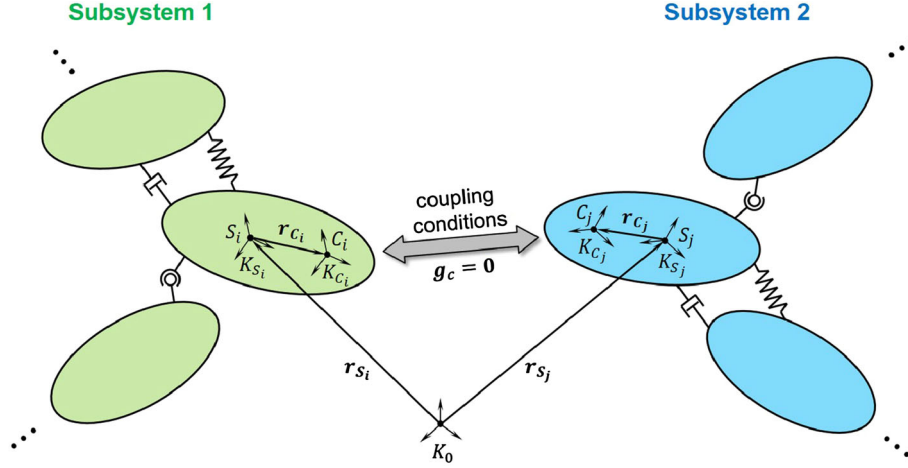


Fig. 5 Body i of subsystem 1 coupled to body j of subsystem 2 (coupling points C_i and C_j)

corrected state variables

$$\begin{aligned} x_{1,N+1} &= x_{1,N+1}(\tilde{x}_{2,N+1}, \tilde{v}_{2,N+1}), & v_{1,N+1} &= v_{1,N+1}(\tilde{x}_{2,N+1}, \tilde{v}_{2,N+1}), \\ x_{2,N+1} &= x_{2,N+1}(\tilde{x}_{1,N+1}, \tilde{v}_{1,N+1}), & v_{2,N+1} &= v_{2,N+1}(\tilde{x}_{1,N+1}, \tilde{v}_{1,N+1}). \end{aligned} \quad (49)$$

- It should again be stressed that the corrected state variables have been calculated with the help of the linearized coupling conditions (44)–(47). For nonlinear problems, the corrected states from Eq. (49) do in general not fulfill the coupling conditions, i.e., $g_{cx1,N+1}(\tilde{x}_{1,N+1}, \tilde{x}_{2,N+1}, \tilde{v}_{2,N+1}) \neq 0$, $g_{cv1,N+1}(\tilde{v}_{1,N+1}, \tilde{x}_{2,N+1}, \tilde{v}_{2,N+1}) \neq 0$, $g_{cx2,N+1}(\tilde{x}_{1,N+1}, \tilde{v}_{1,N+1}, \tilde{x}_{2,N+1}) \neq 0$ and $g_{cv2,N+1}(\tilde{x}_{1,N+1}, \tilde{v}_{1,N+1}, \tilde{v}_{2,N+1}) \neq 0$. Consistent corrected coupling variables can be determined in a final evaluation by solving

$$\begin{aligned} g_{cx1,N+1}(\tilde{x}_{1,N+1}^{\text{final}}, x_{1,N+1}(\tilde{x}_{2,N+1}, \tilde{v}_{2,N+1})) &= 0, \\ g_{cv1,N+1}(\tilde{v}_{1,N+1}^{\text{final}}, v_{1,N+1}(\tilde{x}_{2,N+1}, \tilde{v}_{2,N+1})) &= 0, \\ g_{cx2,N+1}(\tilde{x}_{2,N+1}^{\text{final}}, x_{2,N+1}(\tilde{x}_{1,N+1}, \tilde{v}_{1,N+1})) &= 0, \\ g_{cv2,N+1}(\tilde{v}_{2,N+1}^{\text{final}}, v_{2,N+1}(\tilde{x}_{1,N+1}, \tilde{v}_{1,N+1})) &= 0 \end{aligned} \quad (50)$$

for $\tilde{x}_{1,N+1}^{\text{final}}$, $\tilde{v}_{1,N+1}^{\text{final}}$, $\tilde{x}_{2,N+1}^{\text{final}}$, $\tilde{v}_{2,N+1}^{\text{final}}$. Using $\tilde{x}_{1,N+1}^{\text{final}}$, $\tilde{v}_{1,N+1}^{\text{final}}$, $\tilde{x}_{2,N+1}^{\text{final}}$, $\tilde{v}_{2,N+1}^{\text{final}}$ from Eq. (50) instead of $\tilde{x}_{1,N+1}$, $\tilde{v}_{1,N+1}$, $\tilde{x}_{2,N+1}$, $\tilde{v}_{2,N+1}$ from Eq. (48) as corrected coupling variables at the macro-time point T_{N+1} may improve the simulation results.

3 Semi-implicit co-simulation approach for general mechanical systems

3.1 Definition of the coupled system

We consider 2 arbitrary mechanical subsystems, where subsystem 1 consists of n_1 rigid bodies and subsystem 2 of n_2 rigid bodies. In general, each subsystem is described by a DAE system. The subsystems are mechanically coupled by means of applied forces/torques. Concretely, marker K_{C_i} of body i belonging to subsystem 1 is connected to marker K_{C_j} of body j belonging to subsystem 2 by an arbitrary nonlinear 6-DOF bushing element, see Fig. 5.

The position vector to the center of mass S_i of body i is denoted by r_{S_i} . K_{S_i} is the body-fixed principal axes system at S_i . The coupling point C_i is defined by the body-fixed vector r_{C_i} . K_{C_i} is a body-fixed system at C_i , the axes of which are assumed to be parallel to those of K_{S_i} . An equivalent notation is used for subsystem 2 ($i \rightarrow j$). The inertial reference frame is indicated by K_0 .

Let \mathbf{a} term an arbitrary vector. Its coordinates with respect to system K_m are denoted by ${}^m\mathbf{a}$. With the transformation matrix ${}^{nm}\mathbf{T}$, the vector coordinates can be transformed from system K_m to system K_n , i.e., ${}^n\mathbf{a} = {}^{nm}\mathbf{T} {}^m\mathbf{a}$. In this paper, we use absolute coordinates to describe multibody systems [10,21]. Position and orientation of

an arbitrary rigid body q are described by the three coordinates of the center of mass ${}^0\mathbf{r}_{S_q}$ and by three rotation parameters collected in the vector $\boldsymbol{\gamma}_q \in \mathbb{R}^3$ (e.g., by 3 Euler angles). The coordinates of the velocity of the center of mass S_q with respect to K_0 are given by ${}^0\dot{\mathbf{v}}_{S_q} = {}^0\dot{\mathbf{r}}_{S_q}$. The coordinates of the angular velocity with respect to the body-fixed system K_{S_q} are related to the time derivative of the rotation parameters by the general expression $\dot{\boldsymbol{\gamma}}_q = \mathbf{B}(\boldsymbol{\gamma}_q)^q \boldsymbol{\omega}_q$. Using Euler angles $\boldsymbol{\gamma}_q = (\psi_q \ \theta_q \ \phi_q)^T$ as rotation parameters, for instance, the matrix $\mathbf{B}(\boldsymbol{\gamma}_q) \in \mathbb{R}^{3 \times 3}$ is given by

$$\mathbf{B} = \frac{1}{\sin \theta_q} \begin{pmatrix} \sin \phi_q & \cos \phi_q & 0 \\ \sin \theta_q \cos \phi_q & -\sin \theta_q \sin \phi_q & 0 \\ -\cos \theta_q \sin \phi_q & -\cos \theta_q \cos \phi_q & \sin \theta_q \end{pmatrix}. \quad (51)$$

Next, we define some auxiliary vectors. The vector $\mathbf{z}_i = (z_{i1} \ z_{i2} \ \dots \ z_{i12})^T = ({}^0\mathbf{r}_{S_i}^T \ \boldsymbol{\gamma}_i^T \ {}^0\mathbf{v}_{S_i}^T \ {}^i\boldsymbol{\omega}_i^T)^T \in \mathbb{R}^{12}$ and the vector $\mathbf{z}_j = (z_{j1} \ z_{j2} \ \dots \ z_{j12})^T = ({}^0\mathbf{r}_{S_j}^T \ \boldsymbol{\gamma}_j^T \ {}^0\mathbf{v}_{S_j}^T \ {}^j\boldsymbol{\omega}_j^T)^T \in \mathbb{R}^{12}$ collect the position and velocity coordinates of the coupling bodies i and j . The vector $\mathbf{z}_c = (\mathbf{z}_i^T \ \mathbf{z}_j^T)^T \in \mathbb{R}^{24}$ contains the position and velocity coordinates of both coupling bodies. The vector $\hat{\mathbf{z}}_1 \in \mathbb{R}^{12 \cdot n_1}$ collects the position and velocity coordinates of all bodies of subsystem 1 and the vector $\hat{\mathbf{z}}_2 \in \mathbb{R}^{12 \cdot n_2}$ the position and velocity coordinates of all bodies of subsystem 2.

Now, we formulate the Newton–Euler equations for the coupling bodies i and j . Evaluating Newton's law in K_0 and Euler's law in the body-fixed system K_{S_i} and K_{S_j} , respectively, yields

Coupling body i (subsystem 1):

$$\begin{aligned} {}^0\dot{\mathbf{r}}_{S_i} &= {}^0\mathbf{v}_{S_i}, & m_i {}^0\dot{\mathbf{v}}_{S_i} &= {}^0\mathbf{F}_{a_i}(\hat{\mathbf{z}}_1, t) + {}^0\mathbf{F}_{r_i} + {}^0\mathbf{F}_{c_i}(\mathbf{z}_c), \\ \dot{\boldsymbol{\gamma}}_i &= \mathbf{B}(\boldsymbol{\gamma}_i)^i \boldsymbol{\omega}_i, & {}^i\mathbf{J}_i^i \dot{\boldsymbol{\omega}}_i + {}^i\boldsymbol{\omega}_i \times {}^i\mathbf{J}_i^i \boldsymbol{\omega}_i &= {}^i\mathbf{M}_{a_i}(\hat{\mathbf{z}}_1, t) + {}^i\mathbf{M}_{r_i} + {}^i\mathbf{M}_{c_i}(\mathbf{z}_c), \end{aligned} \quad (52)$$

Coupling body j (subsystem 2):

$$\begin{aligned} {}^0\dot{\mathbf{r}}_{S_j} &= {}^0\mathbf{v}_{S_j}, & m_j {}^0\dot{\mathbf{v}}_{S_j} &= {}^0\mathbf{F}_{a_j}(\hat{\mathbf{z}}_2, t) + {}^0\mathbf{F}_{r_j} + {}^0\mathbf{F}_{c_j}(\mathbf{z}_c), \\ \dot{\boldsymbol{\gamma}}_j &= \mathbf{B}(\boldsymbol{\gamma}_j)^j \boldsymbol{\omega}_j, & {}^j\mathbf{J}_j^j \dot{\boldsymbol{\omega}}_j + {}^j\boldsymbol{\omega}_j \times {}^j\mathbf{J}_j^j \boldsymbol{\omega}_j &= {}^j\mathbf{M}_{a_j}(\hat{\mathbf{z}}_2, t) + {}^j\mathbf{M}_{r_j} + {}^j\mathbf{M}_{c_j}(\mathbf{z}_c). \end{aligned} \quad (53)$$

In the above equations, m_i denotes the mass of body i and ${}^i\mathbf{J}_i$ the matrix with the constant coordinates of the inertia tensor with respect to K_{S_i} . ${}^0\mathbf{F}_{a_i}$ and ${}^i\mathbf{M}_{a_i}$ denote externally applied forces/torques. ${}^0\mathbf{F}_{r_i}$ and ${}^i\mathbf{M}_{r_i}$ represent reaction forces/torques resulting from algebraic constraints in subsystem 1. ${}^0\mathbf{F}_{c_i}$ and ${}^i\mathbf{M}_{c_i}$ are the coupling forces/torques. For subsystem 2, the notation is equivalent ($i \rightarrow j$).

3.2 Coupling of subsystems: concept of flexible joints

In order to describe quite general coupling elements, we use the concept of *flexible joints*, which may also be interpreted as a kind of penalty method. Therefore, we firstly define *fundamental flexible joints*. By combining different fundamental flexible joints, rather general coupling (bushing) elements can be realized.

3.2.1 Flexible atpoint joint (flexible spherical joint)

The first fundamental flexible joint is the *flexible atpoint joint*, described by three scalar coupling conditions collected in the coupling vector $\mathbf{g}_{ca} \in \mathbb{R}^3$. The *linear flexible atpoint joint* is defined by the coupling conditions

$$\mathbf{g}_{ca} := \lambda_{ca} - \mathbf{C} \cdot [(\mathbf{r}_{S_i} + \mathbf{r}_{C_i}) - (\mathbf{r}_{S_j} + \mathbf{r}_{C_j})] - \mathbf{D} \cdot \frac{d}{dt} \{[(\mathbf{r}_{S_i} + \mathbf{r}_{C_i}) - (\mathbf{r}_{S_j} + \mathbf{r}_{C_j})]\} = \mathbf{0}. \quad (54)$$

The diagonal matrix $\mathbf{C} = \text{diag}(c_x, c_y, c_z)$ contains three spring constants and the diagonal matrix $\mathbf{D} = \text{diag}(d_x, d_y, d_z)$ three damping coefficients (non-diagonal elements are neglected for the reason of a clear representation). d/dt terms the total time derivative with respect to K_0 . Note that λ_{ca} can physically be interpreted as a coupling (penalty) force, which is proportional to the relative displacement and to the relative

velocity of the coupling points C_i and C_j . With the three coupling variables ${}^0\lambda_{ca} = ({}^0\lambda_{ca_x} \ {}^0\lambda_{ca_y} \ {}^0\lambda_{ca_z})^T$, evaluation of Eq. (54) with respect to the system K_0 yields

$$\begin{aligned} \mathbf{g}_{ca} := & {}^0\lambda_{ca} - \mathbf{C} \cdot \left[\left({}^0\mathbf{r}_{S_i} + {}^{0i}\mathbf{T}(\boldsymbol{\gamma}_i)^i\mathbf{r}_{C_i} \right) - \left({}^0\mathbf{r}_{S_j} + {}^{0j}\mathbf{T}(\boldsymbol{\gamma}_j)^j\mathbf{r}_{C_j} \right) \right] \\ & + \mathbf{D} \cdot \left[\left({}^0\mathbf{v}_{S_i} + {}^{0i}\mathbf{T}(\boldsymbol{\gamma}_i)^i\boldsymbol{\omega}_i \times {}^{0i}\mathbf{T}(\boldsymbol{\gamma}_i)^i\mathbf{r}_{C_i} \right) - \left({}^0\mathbf{v}_{S_j} + {}^{0j}\mathbf{T}(\boldsymbol{\gamma}_j)^j\boldsymbol{\omega}_j \times {}^{0j}\mathbf{T}(\boldsymbol{\gamma}_j)^j\mathbf{r}_{C_j} \right) \right] = \mathbf{0}. \end{aligned} \quad (55)$$

The *nonlinear flexible atpoint joint* is generally defined by the three coupling conditions

$$\mathbf{g}_{ca} := {}^0\lambda_{ca} - {}^0f_{ca}(z_c) = \mathbf{0}, \quad (56)$$

where ${}^0f_{ca}$ denotes an arbitrary vector function of the relative displacement and the relative velocity of the coupling points C_i and C_j .

Connecting C_i and C_j by a flexible atpoint joint, the following coupling forces and torques are generated, see Eqs. (52) and (53)

$$\begin{aligned} {}^0\mathbf{F}_{ci} &= {}^0\lambda_{ca}, \quad {}^i\mathbf{M}_{ci} = {}^i\mathbf{r}_{C_i} \times {}^{i0}\mathbf{T}(\boldsymbol{\gamma}_i){}^0\lambda_{ca}, \\ {}^0\mathbf{F}_{cj} &= -{}^0\lambda_{ca}, \quad {}^j\mathbf{M}_{cj} = -{}^j\mathbf{r}_{C_j} \times {}^{j0}\mathbf{T}(\boldsymbol{\gamma}_j){}^0\lambda_{ca}. \end{aligned} \quad (57)$$

3.2.2 Flexible inplane joint

The second fundamental flexible joint is the *flexible inplane joint*, described by 1 scalar coupling condition. The *linear flexible inplane joint* is defined by the coupling condition

$$g_{cd} := \lambda_{cd} - c \cdot [(\mathbf{r}_{S_i} + \mathbf{r}_{C_i}) - (\mathbf{r}_{S_j} + \mathbf{r}_{C_j})] \cdot \mathbf{e}_j - d \cdot \frac{d}{dt} \{ [(\mathbf{r}_{S_i} + \mathbf{r}_{C_i}) - (\mathbf{r}_{S_j} + \mathbf{r}_{C_j})] \cdot \mathbf{e}_j \} = 0. \quad (58)$$

\mathbf{e}_j denotes an arbitrary unit vector fixed at body j . c is a spring constant and d a damping coefficient. λ_{cd} can be interpreted as a force, which is proportional to the penetration and to the penetration velocity of C_i into the plane with normal vector \mathbf{e}_j fixed at C_j . For the reason of a concise representation, the time derivative for the calculation of the penetration velocity is not carried out explicitly. Decomposing the vectors in Eq. (58) with respect to the system K_0 yields

$$\begin{aligned} g_{cd} := & \lambda_{cd} - c \cdot \left[\left({}^0\mathbf{r}_{S_i} + {}^{0i}\mathbf{T}(\boldsymbol{\gamma}_i)^i\mathbf{r}_{C_i} \right) - \left({}^0\mathbf{r}_{S_j} + {}^{0j}\mathbf{T}(\boldsymbol{\gamma}_j)^j\mathbf{r}_{C_j} \right) \right] \cdot {}^{0j}\mathbf{T}(\boldsymbol{\gamma}_j)^j\mathbf{e}_j \\ & - d \cdot \frac{d}{dt} \left\{ \left[\left({}^0\mathbf{r}_{S_i} + {}^{0i}\mathbf{T}(\boldsymbol{\gamma}_i)^i\mathbf{r}_{C_i} \right) - \left({}^0\mathbf{r}_{S_j} + {}^{0j}\mathbf{T}(\boldsymbol{\gamma}_j)^j\mathbf{r}_{C_j} \right) \right] \cdot {}^{0j}\mathbf{T}(\boldsymbol{\gamma}_j)^j\mathbf{e}_j \right\} = 0. \end{aligned} \quad (59)$$

The *nonlinear flexible inplane joint* is defined by the coupling condition

$$g_{cd} := \lambda_{cd} - f_{cd}(z_c) = 0, \quad (60)$$

where f_{cd} denotes an arbitrary function of the penetration and the penetration velocity of C_i into the body-fixed plane at C_j .

Connecting C_i und C_j by a flexible inplane joint yields the following coupling forces and torques

$$\begin{aligned} {}^0\mathbf{F}_{ci} &= {}^{0j}\mathbf{T}(\boldsymbol{\gamma}_j)^j\mathbf{e}_j \lambda_{cd}, \quad {}^i\mathbf{M}_{ci} = {}^i\mathbf{r}_{C_i} \times {}^{ij}\mathbf{T}(\boldsymbol{\gamma}_i, \boldsymbol{\gamma}_j)^j\mathbf{e}_j \lambda_{cd}, \\ {}^0\mathbf{F}_{cj} &= -{}^{0j}\mathbf{T}(\boldsymbol{\gamma}_j)^j\mathbf{e}_j \lambda_{cd}, \quad {}^j\mathbf{M}_{cj} = {}^j\mathbf{e}_j \times {}^{j0}\mathbf{T}(\boldsymbol{\gamma}_j) \left({}^0\mathbf{r}_{S_i} + {}^{0i}\mathbf{T}(\boldsymbol{\gamma}_i)^i\mathbf{r}_{C_i} - {}^0\mathbf{r}_{S_j} \right) \lambda_{cd}. \end{aligned} \quad (61)$$

The contact situation for the flexible inplane joint is illustrated in Fig. 6. The coupling force ${}^0\mathbf{F}_{ci}$ is acting on body i at point C_i . The reaction force ${}^0\mathbf{F}_{cj}$ is acting on body j at point \bar{C}_j (projection of C_i onto the plane defined by C_j and \mathbf{e}_j). The direction of the coupling forces is defined by \mathbf{e}_j . Note that for calculating the torque of ${}^0\mathbf{F}_{ci}$ with respect to S_j , the force can be moved along its line of action to the point C_i .

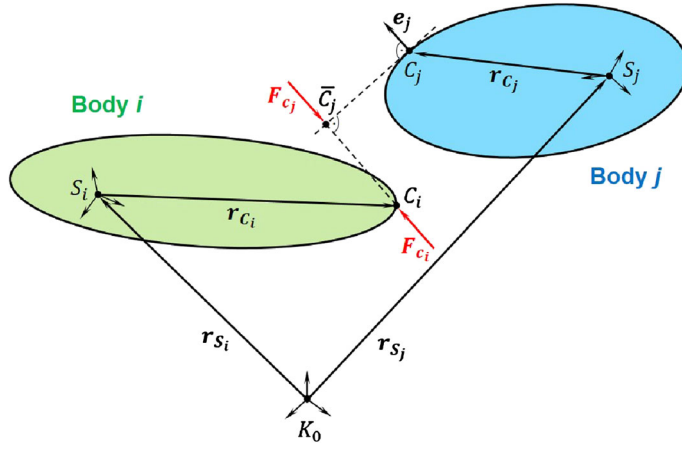


Fig. 6 Flexible inplane joint: geometry and coupling forces

3.2.3 Flexible perpendicular joint

The third fundamental flexible joint is the *flexible perpendicular joint*. The *linear flexible perpendicular joint* is described by the coupling condition

$$g_{cp} := \lambda_{cp} - c \cdot (\mathbf{e}_i \cdot \mathbf{e}_j) - d \cdot \frac{d}{dt} \{ \mathbf{e}_i \cdot \mathbf{e}_j \} = 0. \quad (62)$$

\mathbf{e}_i and \mathbf{e}_j denote arbitrary unit vectors fixed at body i and body j , respectively. c represents a torsional spring constant and d a torsional damping coefficient. Hence, λ_{cp} can be interpreted as a torque, the elastic part of which is proportional to the cosine of the angle between \mathbf{e}_i and \mathbf{e}_j (usually \mathbf{e}_i and \mathbf{e}_j are assumed to be orthogonal in the stress-free reference configuration). The second term represents a torsional damping torque. Evaluating the vectors in Eq. (62) with respect to the system K_0 yields

$$g_{cp} := \lambda_{cp} - c \cdot \left({}^{0i} \mathbf{T}(\gamma_i)^i \mathbf{e}_i \cdot {}^{0j} \mathbf{T}(\gamma_j)^j \mathbf{e}_j \right) - d \cdot \frac{d}{dt} \left\{ {}^{0i} \mathbf{T}(\gamma_i)^i \mathbf{e}_i \cdot {}^{0j} \mathbf{T}(\gamma_j)^j \mathbf{e}_j \right\} = 0. \quad (63)$$

The *nonlinear flexible perpendicular joint* is defined by the coupling condition

$$g_{cp} := \lambda_{cp} - f_{cp} (\gamma_i, {}^i \omega_i, \gamma_j, {}^j \omega_j) = 0, \quad (64)$$

where f_{cp} denotes an arbitrary function of the cosine of the angle between \mathbf{e}_i and \mathbf{e}_j and its time derivative.

Connecting C_i and C_j by a flexible perpendicular joint, the coupling forces and torques read as

$$\begin{aligned} {}^0 \mathbf{F}_{ci} &= \mathbf{0}, & {}^i \mathbf{M}_{ci} &= {}^i \mathbf{e}_i \times {}^{ij} \mathbf{T}(\gamma_i, \gamma_j)^j \mathbf{e}_j \lambda_{cp}, \\ {}^0 \mathbf{F}_{cj} &= \mathbf{0}, & {}^j \mathbf{M}_{cj} &= {}^j \mathbf{e}_j \times {}^{ji} \mathbf{T}(\gamma_i, \gamma_j)^i \mathbf{e}_i \lambda_{cp}. \end{aligned} \quad (65)$$

It should be stressed that the cross product vanishes if \mathbf{e}_i and \mathbf{e}_j become parallel. In this singular position, the torques are not defined and special techniques have to be applied to circumvent the singularity (according to the handling of singularities in connection with Euler angles, for instance). It should further be mentioned that using high coupling stiffnesses (penalty stiffnesses), the angle between \mathbf{e}_i and \mathbf{e}_j almost remains constant ($\approx \pi/2$) so that the torque calculation according to Eq. (65) is appropriate. For soft coupling stiffnesses, other formulations may be more useful, e.g., scaling the torques in Eq. (65) by $(\mathbf{e}_i \times \mathbf{e}_j)^{-1}$ so that λ_{cp} reflects the magnitude of the torques.

3.2.4 Combination of fundamental flexible joints

Combining different fundamental flexible joints, further flexible joints can be generated, e.g., the *flexible universal joint* (1 atpoint joint + 1 perpendicular joint), the *flexible revolute joint* (1 atpoint joint + 2 perpendicular joints), the *flexible translational joint* (3 perpendicular joints + 2 inplane joints), the *flexible cylindrical joint* (2 perpendicular joints + 2 inplane joints), the *flexible planar joint* (2 perpendicular joints + 1 inplane joint), the *flexible inline joint* (2 inplane joints) and the *flexible orientation joint* (3 perpendicular joints), see [10].

3.3 Force/force-coupling

When the force/force-coupling approach is applied, the coupling variables ${}^0\lambda_{ca}$, λ_{cd} and λ_{cp} are used in both subsystems.

3.3.1 Flexible atpoint joint

Using a force/force-coupling approach and connecting body i and body j by a flexible atpoint joint, the coupling forces/torques acting on bodies i and j as well as the three scalar coupling conditions read as

$$\begin{aligned} {}^0\mathbf{F}_{ci} &= {}^0\lambda_{ca}, \quad {}^i\mathbf{M}_{ci} = {}^i\mathbf{r}_{Ci} \times {}^{i0}\mathbf{T}(\boldsymbol{\gamma}_i) {}^0\lambda_{ca}, \\ {}^0\mathbf{F}_{cj} &= -{}^0\lambda_{ca}, \quad {}^j\mathbf{M}_{cj} = -{}^j\mathbf{r}_{Cj} \times {}^{j0}\mathbf{T}(\boldsymbol{\gamma}_j) {}^0\lambda_{ca}, \\ \mathbf{g}_{ca} &:= {}^0\lambda_{ca} - {}^0f_{ca}(z_c) = \mathbf{0}. \end{aligned} \quad (66)$$

Eqs. (52), (53) and (66) represent the equations of motion for the coupling bodies i and j for the case that the bodies are connected by a flexible atpoint joint.

3.3.2 Flexible inplane joint

For the flexible inplane joint, the coupling forces/torques and the 10 scalar coupling conditions are given by

$$\begin{aligned} {}^0\mathbf{F}_{ci} &= {}^0j\mathbf{T}(\tilde{\boldsymbol{\gamma}}_j) {}^j\mathbf{e}_j \lambda_{cd}, \quad {}^i\mathbf{M}_{ci} = {}^i\mathbf{r}_{Ci} \times {}^{ij}\mathbf{T}(\boldsymbol{\gamma}_i, \tilde{\boldsymbol{\gamma}}_j) {}^j\mathbf{e}_j \lambda_{cd}, \\ {}^0\mathbf{F}_{cj} &= -{}^0j\mathbf{T}(\boldsymbol{\gamma}_j) {}^j\mathbf{e}_j \lambda_{cd}, \quad {}^j\mathbf{M}_{cj} = {}^j\mathbf{e}_j \times {}^{j0}\mathbf{T}(\boldsymbol{\gamma}_j) \left({}^0\tilde{\mathbf{r}}_{Si} + {}^{0i}\mathbf{T}(\tilde{\boldsymbol{\gamma}}_i) {}^i\mathbf{r}_{Ci} - {}^0\mathbf{r}_{Sj} \right) \lambda_{cd}, \\ g_{cd} &:= \lambda_{cd} - f_{cd}(z_c) = 0, \quad \mathbf{g}_{cr_i} := {}^0\tilde{\mathbf{r}}_{Si} - {}^0\mathbf{r}_{Si} = \mathbf{0}, \quad \mathbf{g}_{c\gamma_i} := \tilde{\boldsymbol{\gamma}}_i - \boldsymbol{\gamma}_i = \mathbf{0}, \\ \mathbf{g}_{c\gamma_j} &:= \tilde{\boldsymbol{\gamma}}_j - \boldsymbol{\gamma}_j = \mathbf{0}. \end{aligned} \quad (67)$$

Eq. (67) together with Eqs. (52) and (53) are the equations of motion for the coupling bodies i and j for the case that the bodies are connected by a flexible inplane joint. Applying a co-simulation approach, the subsystems are integrated independently from T_N to T_{N+1} . Therefore, the state variables z_j are not available in subsystem 1, and the state variables z_i are not accessible in subsystem 2. For that reason, the state variables $\boldsymbol{\gamma}_j$ are replaced by the additional coupling variables $\tilde{\boldsymbol{\gamma}}_j$ in subsystem 1. In subsystem 2, the state variables ${}^0\mathbf{r}_{Si}$ and $\boldsymbol{\gamma}_i$ are replaced by the additional coupling variables ${}^0\tilde{\mathbf{r}}_{Si}$ and $\tilde{\boldsymbol{\gamma}}_i$. Due to the additional coupling variables, the additional coupling conditions \mathbf{g}_{cr_i} , $\mathbf{g}_{c\gamma_i}$ and $\mathbf{g}_{c\gamma_j}$ (representing nine scalar coupling conditions) have to be added to the decomposed system.

3.3.3 Flexible perpendicular joint

Applying a flexible perpendicular joint, the coupling forces/torques and the seven scalar coupling conditions are given by

$$\begin{aligned} {}^0\mathbf{F}_{ci} &= \mathbf{0}, \quad {}^i\mathbf{M}_{ci} = {}^i\mathbf{e}_i \times {}^{ij}\mathbf{T}(\boldsymbol{\gamma}_i, \tilde{\boldsymbol{\gamma}}_j) {}^j\mathbf{e}_j \lambda_{cp}, \\ {}^0\mathbf{F}_{cj} &= \mathbf{0}, \quad {}^j\mathbf{M}_{cj} = {}^j\mathbf{e}_j \times {}^{ji}\mathbf{T}(\tilde{\boldsymbol{\gamma}}_i, \boldsymbol{\gamma}_j) {}^i\mathbf{e}_i \lambda_{cp}, \\ g_{cp} &:= \lambda_{cp} - f_{cp} (\boldsymbol{\gamma}_i, {}^i\omega_i, \boldsymbol{\gamma}_j, {}^j\omega_j) = 0, \quad \mathbf{g}_{c\gamma_i} := \tilde{\boldsymbol{\gamma}}_i - \boldsymbol{\gamma}_i = \mathbf{0}, \quad \mathbf{g}_{c\gamma_j} := \tilde{\boldsymbol{\gamma}}_j - \boldsymbol{\gamma}_j = \mathbf{0}. \end{aligned} \quad (68)$$

Eqs. (52), (53) and (68) represent the equations of motion for the coupling bodies i and j . For the flexible perpendicular joint, six additional coupling variables ($\tilde{\boldsymbol{\gamma}}_i$ and $\tilde{\boldsymbol{\gamma}}_j$) and six additional scalar coupling conditions ($\mathbf{g}_{c\gamma_i}$ and $\mathbf{g}_{c\gamma_j}$) have to be defined. Note that in ‘‘Appendix C’’ an alternative formulation for the flexible perpendicular joint is presented.

3.4 Force/displacement-coupling

The general idea of the force/displacement-coupling approach is to replace the coupling variables ${}^0\lambda_{ca}$, λ_{cd} and λ_{cp} in subsystem 2 by means of the coupling conditions \mathbf{g}_{ca} , \mathbf{g}_{cd} and \mathbf{g}_{cp} . As a consequence, further coupling variables and coupling conditions have to be defined.

3.4.1 Flexible atpoint joint

If body i and body j are coupled by a flexible atpoint joint, the coupling forces/torques and the altogether 15 scalar coupling conditions read as follows

$$\begin{aligned} {}^0\mathbf{F}_{ci} &= {}^0\lambda_{ca}, \quad {}^i\mathbf{M}_{ci} = {}^i\mathbf{r}_{Ci} \times {}^{i0}\mathbf{T}(\boldsymbol{\gamma}_i) {}^0\lambda_{ca}, \\ {}^0\mathbf{F}_{cj} &= -{}^0\mathbf{f}_{ca}(\tilde{\mathbf{u}}_i, \mathbf{z}_j), \quad {}^j\mathbf{M}_{cj} = -{}^j\mathbf{r}_{Cj} \times {}^{j0}\mathbf{T}(\boldsymbol{\gamma}_j) {}^0\mathbf{f}_{ca}(\tilde{\mathbf{u}}_i, \mathbf{z}_j), \\ \mathbf{g}_{ca} &:= {}^0\lambda_{ca} - {}^0\mathbf{f}_{ca}(\mathbf{z}_c) = \mathbf{0}, \quad \mathbf{g}_{cr_i} := {}^0\tilde{\mathbf{r}}_{Si} - {}^0\mathbf{r}_{Si} = \mathbf{0}, \quad \mathbf{g}_{c\gamma_i} := \tilde{\boldsymbol{\gamma}}_i - \boldsymbol{\gamma}_i = \mathbf{0}, \\ \mathbf{g}_{cv_i} &:= {}^0\tilde{\mathbf{v}}_{Si} - {}^0\mathbf{v}_{Si} = \mathbf{0}, \quad \mathbf{g}_{c\omega_i} := {}^i\tilde{\boldsymbol{\omega}}_i - {}^i\boldsymbol{\omega}_i = \mathbf{0}. \end{aligned} \quad (69)$$

The coupling variables for subsystem 2 are formally collected in the coupling vector $\tilde{\mathbf{u}}_i = \left({}^0\tilde{\mathbf{r}}_{Si}^T \ \tilde{\boldsymbol{\gamma}}_i^T \ {}^0\tilde{\mathbf{v}}_{Si}^T \ {}^i\tilde{\boldsymbol{\omega}}_i^T \right)^T$, see Sect. 3.6.

3.4.2 Flexible inplane joint

Making use of a flexible inplane joint to connect bodies i and j , 16 scalar coupling conditions have to be considered. Together with the coupling forces and torques, one gets

$$\begin{aligned} {}^0\mathbf{F}_{ci} &= {}^0j\mathbf{T}(\tilde{\boldsymbol{\gamma}}_j) {}^j\mathbf{e}_j \lambda_{cd}, \quad {}^i\mathbf{M}_{ci} = {}^i\mathbf{r}_{Ci} \times {}^{ij}\mathbf{T}(\boldsymbol{\gamma}_i, \tilde{\boldsymbol{\gamma}}_j) {}^j\mathbf{e}_j \lambda_{cd}, \\ {}^0\mathbf{F}_{cj} &= -{}^0j\mathbf{T}(\boldsymbol{\gamma}_j) {}^j\mathbf{e}_j f_{cd}(\tilde{\mathbf{u}}_i, \mathbf{z}_j), \\ {}^j\mathbf{M}_{cj} &= {}^j\mathbf{e}_j \times {}^{j0}\mathbf{T}(\boldsymbol{\gamma}_j) \left({}^0\tilde{\mathbf{r}}_{Si} + {}^{0i}\mathbf{T}(\tilde{\boldsymbol{\gamma}}_i) {}^i\mathbf{r}_{Ci} - {}^0\mathbf{r}_{Sj} \right) f_{cd}(\tilde{\mathbf{u}}_i, \mathbf{z}_j), \\ g_{cd} &:= \lambda_{cd} - f_{cd}(\mathbf{z}_c) = 0, \quad \mathbf{g}_{cr_i} := {}^0\tilde{\mathbf{r}}_{Si} - {}^0\mathbf{r}_{Si} = \mathbf{0}, \quad \mathbf{g}_{c\gamma_i} := \tilde{\boldsymbol{\gamma}}_i - \boldsymbol{\gamma}_i = \mathbf{0}, \\ \mathbf{g}_{cv_i} &:= {}^0\tilde{\mathbf{v}}_{Si} - {}^0\mathbf{v}_{Si} = \mathbf{0}, \quad \mathbf{g}_{c\omega_i} := {}^i\tilde{\boldsymbol{\omega}}_i - {}^i\boldsymbol{\omega}_i = \mathbf{0}, \quad \mathbf{g}_{c\gamma_j} := \tilde{\boldsymbol{\gamma}}_j - \boldsymbol{\gamma}_j = \mathbf{0}, \end{aligned} \quad (70)$$

where the vector $\tilde{\mathbf{u}}_i = \left({}^0\tilde{\mathbf{r}}_{Si}^T \ \tilde{\boldsymbol{\gamma}}_i^T \ {}^0\tilde{\mathbf{v}}_{Si}^T \ {}^i\tilde{\boldsymbol{\omega}}_i^T \right)^T$ contains the coupling variables for subsystem 2.

3.4.3 Flexible perpendicular joint

If the subsystems are coupled by a flexible perpendicular joint, the coupling forces/torques as well as the 10 scalar coupling conditions are given by

$$\begin{aligned} {}^0\mathbf{F}_{ci} &= \mathbf{0}, \quad {}^i\mathbf{M}_{ci} = {}^i\mathbf{e}_i \times {}^{ij}\mathbf{T}(\boldsymbol{\gamma}_i, \tilde{\boldsymbol{\gamma}}_j) {}^j\mathbf{e}_j \lambda_{cp}, \\ {}^0\mathbf{F}_{cj} &= \mathbf{0}, \quad {}^j\mathbf{M}_{cj} = {}^j\mathbf{e}_j \times {}^{ji}\mathbf{T}(\tilde{\boldsymbol{\gamma}}_i, \boldsymbol{\gamma}_j) {}^i\mathbf{e}_i f_{cp}(\tilde{\mathbf{u}}_i, \mathbf{z}_j), \\ g_{cp} &:= \lambda_{cp} - f_{cp}(\boldsymbol{\gamma}_i, {}^i\boldsymbol{\omega}_i, \boldsymbol{\gamma}_j, {}^j\boldsymbol{\omega}_j) = 0, \quad \mathbf{g}_{c\gamma_i} := \tilde{\boldsymbol{\gamma}}_i - \boldsymbol{\gamma}_i = \mathbf{0}, \\ \mathbf{g}_{c\omega_i} &:= {}^i\tilde{\boldsymbol{\omega}}_i - {}^i\boldsymbol{\omega}_i = \mathbf{0}, \quad \mathbf{g}_{c\gamma_j} := \tilde{\boldsymbol{\gamma}}_j - \boldsymbol{\gamma}_j = \mathbf{0} \end{aligned} \quad (71)$$

with $\tilde{\mathbf{u}}_i = \left(\tilde{\boldsymbol{\gamma}}_i^T \ {}^i\tilde{\boldsymbol{\omega}}_i^T \right)^T$.

3.5 Displacement/displacement-coupling

Using the displacement/displacement-coupling approach, the coupling variables ${}^0\lambda_{ca}$, λ_{cd} and λ_{cp} are replaced in both subsystems by means of the coupling conditions \mathbf{g}_{ca} , \mathbf{g}_{cd} and \mathbf{g}_{cp} .

3.5.1 Flexible atpoint joint

For the case that body i and body j are coupled by a flexible atpoint joint, 24 scalar coupling conditions have to be formulated. The coupling forces/torques and the coupling conditions are given by

$$\begin{aligned} {}^0\mathbf{F}_{ci} &= {}^0\mathbf{f}_{ca}(z_i, \tilde{\mathbf{u}}_j), \quad {}^i\mathbf{M}_{ci} = {}^i\mathbf{r}_{Ci} \times {}^{i0}\mathbf{T}(\boldsymbol{\gamma}_i) {}^0\mathbf{f}_{ca}(z_i, \tilde{\mathbf{u}}_j), \\ {}^0\mathbf{F}_{cj} &= -{}^0\mathbf{f}_{ca}(\tilde{\mathbf{u}}_i, z_j), \quad {}^j\mathbf{M}_{cj} = -{}^j\mathbf{r}_{Cj} \times {}^{j0}\mathbf{T}(\boldsymbol{\gamma}_j) {}^0\mathbf{f}_{ca}(\tilde{\mathbf{u}}_i, z_j), \\ \mathbf{g}_{cri} &:= {}^0\tilde{\mathbf{r}}_{S_i} - {}^0\mathbf{r}_{S_i} = \mathbf{0}, \quad \mathbf{g}_{c\gamma_i} := \tilde{\boldsymbol{\gamma}}_i - \boldsymbol{\gamma}_i = \mathbf{0}, \quad \mathbf{g}_{cv_i} := {}^0\tilde{\mathbf{v}}_{S_i} - {}^0\mathbf{v}_{S_i} = \mathbf{0}, \\ \mathbf{g}_{c\omega_i} &:= {}^i\tilde{\boldsymbol{\omega}}_i - {}^i\boldsymbol{\omega}_i = \mathbf{0}, \quad \mathbf{g}_{cr_j} := {}^0\tilde{\mathbf{r}}_{S_j} - {}^0\mathbf{r}_{S_j} = \mathbf{0}, \quad \mathbf{g}_{c\gamma_j} := \tilde{\boldsymbol{\gamma}}_j - \boldsymbol{\gamma}_j = \mathbf{0}, \\ \mathbf{g}_{cv_j} &:= {}^0\tilde{\mathbf{v}}_{S_j} - {}^0\mathbf{v}_{S_j} = \mathbf{0}, \quad \mathbf{g}_{c\omega_j} := {}^j\tilde{\boldsymbol{\omega}}_j - {}^j\boldsymbol{\omega}_j = \mathbf{0} \end{aligned} \quad (72)$$

with the coupling vectors $\tilde{\mathbf{u}}_i = \left({}^0\tilde{\mathbf{r}}_{S_i}^T \ \tilde{\boldsymbol{\gamma}}_i^T \ {}^0\tilde{\mathbf{v}}_{S_i}^T \ {}^i\tilde{\boldsymbol{\omega}}_i^T\right)^T$ and $\tilde{\mathbf{u}}_j = \left({}^0\tilde{\mathbf{r}}_{S_j}^T \ \tilde{\boldsymbol{\gamma}}_j^T \ {}^0\tilde{\mathbf{v}}_{S_j}^T \ {}^j\tilde{\boldsymbol{\omega}}_j^T\right)^T$.

3.5.2 Flexible inplane joint

Applying a flexible inplane joint, the coupling forces/torques and the 24 scalar coupling conditions are determined by

$$\begin{aligned} {}^0\mathbf{F}_{ci} &= {}^{0j}\mathbf{T}(\tilde{\boldsymbol{\gamma}}_j) {}^j\mathbf{e}_j f_{cd}(z_i, \tilde{\mathbf{u}}_j), \quad {}^i\mathbf{M}_{ci} = {}^i\mathbf{r}_{Ci} \times {}^{ij}\mathbf{T}(\boldsymbol{\gamma}_i, \tilde{\boldsymbol{\gamma}}_j) {}^j\mathbf{e}_j f_{cd}(z_i, \tilde{\mathbf{u}}_j), \\ {}^0\mathbf{F}_{cj} &= -{}^{0j}\mathbf{T}(\boldsymbol{\gamma}_j) {}^j\mathbf{e}_j f_{cd}(\tilde{\mathbf{u}}_i, z_j), \\ {}^j\mathbf{M}_{cj} &= {}^j\mathbf{e}_j \times {}^{j0}\mathbf{T}(\boldsymbol{\gamma}_j) \left({}^0\tilde{\mathbf{r}}_{S_i} + {}^{0i}\mathbf{T}(\tilde{\boldsymbol{\gamma}}_i) {}^i\mathbf{r}_{Ci} - {}^0\mathbf{r}_{S_j}\right) f_{cd}(\tilde{\mathbf{u}}_i, z_j), \\ \mathbf{g}_{cri} &:= {}^0\tilde{\mathbf{r}}_{S_i} - {}^0\mathbf{r}_{S_i} = \mathbf{0}, \quad \mathbf{g}_{c\gamma_i} := \tilde{\boldsymbol{\gamma}}_i - \boldsymbol{\gamma}_i = \mathbf{0}, \quad \mathbf{g}_{cv_i} := {}^0\tilde{\mathbf{v}}_{S_i} - {}^0\mathbf{v}_{S_i} = \mathbf{0}, \\ \mathbf{g}_{c\omega_i} &:= {}^i\tilde{\boldsymbol{\omega}}_i - {}^i\boldsymbol{\omega}_i = \mathbf{0}, \quad \mathbf{g}_{cr_j} := {}^0\tilde{\mathbf{r}}_{S_j} - {}^0\mathbf{r}_{S_j} = \mathbf{0}, \quad \mathbf{g}_{c\gamma_j} := \tilde{\boldsymbol{\gamma}}_j - \boldsymbol{\gamma}_j = \mathbf{0}, \\ \mathbf{g}_{cv_j} &:= {}^0\tilde{\mathbf{v}}_{S_j} - {}^0\mathbf{v}_{S_j} = \mathbf{0}, \quad \mathbf{g}_{c\omega_j} := {}^j\tilde{\boldsymbol{\omega}}_j - {}^j\boldsymbol{\omega}_j = \mathbf{0} \end{aligned} \quad (73)$$

with the coupling vectors $\tilde{\mathbf{u}}_i = \left({}^0\tilde{\mathbf{r}}_{S_i}^T \ \tilde{\boldsymbol{\gamma}}_i^T \ {}^0\tilde{\mathbf{v}}_{S_i}^T \ {}^i\tilde{\boldsymbol{\omega}}_i^T\right)^T$ and $\tilde{\mathbf{u}}_j = \left({}^0\tilde{\mathbf{r}}_{S_j}^T \ \tilde{\boldsymbol{\gamma}}_j^T \ {}^0\tilde{\mathbf{v}}_{S_j}^T \ {}^j\tilde{\boldsymbol{\omega}}_j^T\right)^T$.

3.5.3 Flexible perpendicular joint

By making use of a flexible perpendicular joint, 12 scalar coupling conditions have to be considered. Together with the coupling forces and torques, we have

$$\begin{aligned} {}^0\mathbf{F}_{ci} &= \mathbf{0}, \quad {}^i\mathbf{M}_{ci} = {}^i\mathbf{e}_i \times {}^{ij}\mathbf{T}(\boldsymbol{\gamma}_i, \tilde{\boldsymbol{\gamma}}_j) {}^j\mathbf{e}_j f_{cp}(z_i, \tilde{\mathbf{u}}_j), \\ {}^0\mathbf{F}_{cj} &= \mathbf{0}, \quad {}^j\mathbf{M}_{cj} = {}^j\mathbf{e}_j \times {}^{ji}\mathbf{T}(\tilde{\boldsymbol{\gamma}}_i, \boldsymbol{\gamma}_j) {}^i\mathbf{e}_i f_{cp}(\tilde{\mathbf{u}}_i, z_j), \\ \mathbf{g}_{c\gamma_i} &:= \tilde{\boldsymbol{\gamma}}_i - \boldsymbol{\gamma}_i = \mathbf{0}, \quad \mathbf{g}_{c\omega_i} := {}^i\tilde{\boldsymbol{\omega}}_i - {}^i\boldsymbol{\omega}_i = \mathbf{0}, \\ \mathbf{g}_{c\gamma_j} &:= \tilde{\boldsymbol{\gamma}}_j - \boldsymbol{\gamma}_j = \mathbf{0}, \quad \mathbf{g}_{c\omega_j} := {}^j\tilde{\boldsymbol{\omega}}_j - {}^j\boldsymbol{\omega}_j = \mathbf{0} \end{aligned} \quad (74)$$

with the coupling vectors $\tilde{\mathbf{u}}_i = \left(\tilde{\boldsymbol{\gamma}}_i^T \ {}^i\tilde{\boldsymbol{\omega}}_i^T\right)^T$ and $\tilde{\mathbf{u}}_j = \left(\tilde{\boldsymbol{\gamma}}_j^T \ {}^j\tilde{\boldsymbol{\omega}}_j^T\right)^T$.

3.6 General integration scheme for semi-implicit co-simulation approach

The semi-implicit co-simulation approach is carried out in three steps, which are now compactly described for the force/force-, the force/displacement- and the displacement/displacement-coupling approach. We firstly define some auxiliary vectors. The coupling (input) vector $\tilde{\mathbf{u}}_j = (\tilde{u}_{j1} \ \tilde{u}_{j2} \ \dots \ \tilde{u}_{jn_{\tilde{u}j}})^T \in \mathbb{R}^{n_{\tilde{u}j}}$ collects the $n_{\tilde{u}j}$ coupling variables for the coupling body i ; the coupling (input) vector $\tilde{\mathbf{u}}_i = (\tilde{u}_{i1} \ \tilde{u}_{i2} \ \dots \ \tilde{u}_{in_{\tilde{u}i}})^T \in \mathbb{R}^{n_{\tilde{u}i}}$ contains the $n_{\tilde{u}i}$ coupling variables for the coupling body j . The coupling vectors of both subsystems are

combined in the resultant coupling vector $\tilde{\mathbf{u}}_c = (\tilde{\mathbf{u}}_j^T \ \tilde{\mathbf{u}}_i^T)^T \in \mathbb{R}^{n_{\tilde{u}_j} + n_{\tilde{u}_i}}$. The n_g coupling conditions are formally collected into the vector $\mathbf{g}_c = (g_{c1} \ g_{c2} \ \dots \ g_{cn_g})^T \in \mathbb{R}^{n_g}$. For example, coupling the bodies i and j by a flexible inplane joint (without damping) with a force/force-coupling approach, we get the following coupling variables and coupling conditions: $\tilde{\mathbf{u}}_j = (\lambda_{cd} \ \tilde{\mathbf{y}}_j^T)^T \in \mathbb{R}^4$, $\tilde{\mathbf{u}}_i = (\lambda_{cd} \ ^0\tilde{\mathbf{r}}_{S_i}^T \ \tilde{\mathbf{y}}_i^T)^T \in \mathbb{R}^7$ and $\mathbf{g}_c = (g_{cd} \ g_{cr_i}^T \ g_{c\gamma_i}^T \ g_{c\gamma_j}^T)^T \in \mathbb{R}^{10}$. If we, for instance, connect bodies i and j by a flexible atpoint joint (with damping) and by a flexible perpendicular joint (with damping) with a force/displacement-coupling approach, we get the following coupling variables and coupling conditions: $\tilde{\mathbf{u}}_j = (^0\lambda_{ca}^T \ \lambda_{cp} \ \tilde{\mathbf{y}}_j^T)^T \in \mathbb{R}^7$, $\tilde{\mathbf{u}}_i = (^0\tilde{\mathbf{r}}_{S_i}^T \ \tilde{\mathbf{y}}_i^T \ ^0\tilde{\mathbf{v}}_{S_i}^T \ ^i\tilde{\mathbf{w}}_i^T)^T \in \mathbb{R}^{12}$, and $\mathbf{g}_c = (g_{ca}^T \ g_{cp} \ g_{cr_i}^T \ g_{c\gamma_i}^T \ g_{cv_i}^T \ g_{c\omega_i}^T \ g_{c\gamma_j}^T)^T \in \mathbb{R}^{19}$.

To explain the semi-implicit coupling approach, we consider the general macro-time step from T_N to T_{N+1} . In contrast to Sect. 2, where the coupling variables have been approximated by constant polynomials, we now discuss the general case that the coupling variables $\tilde{\mathbf{u}}_j$ and $\tilde{\mathbf{u}}_i$ are approximated by polynomials of degree k . At the beginning of the macro-time step, the state variables of the subsystems and the coupling variables are assumed to be known

$$\hat{\mathbf{z}}_1(t = T_N) = \hat{\mathbf{z}}_{1,N}, \quad \hat{\mathbf{z}}_2(t = T_N) = \hat{\mathbf{z}}_{2,N}, \quad (75a)$$

$$\tilde{\mathbf{u}}_j(t = T_N) = \tilde{\mathbf{u}}_{j,N}, \quad \tilde{\mathbf{u}}_i(t = T_N) = \tilde{\mathbf{u}}_{i,N}. \quad (75b)$$

Step 1: Predictor step

- For extrapolating the coupling variables in the predictor step, each component of the coupling vectors $\tilde{\mathbf{u}}_j$ and $\tilde{\mathbf{u}}_i$ is approximated by Lagrange polynomials. The $k+1$ sampling points for generating the polynomial of degree k are defined by the macro-time points $T_N, T_{N-1}, \dots, T_{N-k}$. For instance, the predictor polynomial $P_{\lambda_{cd}}^P(t)$ for the coupling variable λ_{cd} in the time interval $[T_N, T_{N+1}]$ is defined by the $k+1$ sampling points $(T_N, \lambda_{cd,N}), (T_{N-1}, \lambda_{cd,N-1}), \dots, (T_{N-k}, \lambda_{cd,N-k})$ and is abbreviated by $P_{\lambda_{cd}}^P[(T_N, \lambda_{cd,N}), (T_{N-1}, \lambda_{cd,N-1}), \dots, (T_{N-k}, \lambda_{cd,N-k}); t]$. The extrapolation polynomials for subsystem 1 and subsystem 2 are formally collected into the vectors $\mathbf{P}_j^P \in \mathbb{R}^{n_{\tilde{u}_j}}$ and $\mathbf{P}_i^P \in \mathbb{R}^{n_{\tilde{u}_i}}$.
- Integration of subsystem 1 and subsystem 2 from T_N to T_{N+1} with initial conditions (75a) and with the predicted (extrapolated) coupling variables

$$\begin{aligned} \tilde{\mathbf{u}}_j^P(t) &= \mathbf{P}_j^P[(T_N, \tilde{\mathbf{u}}_{j,N}), (T_{N-1}, \tilde{\mathbf{u}}_{j,N-1}), \dots, (T_{N-k}, \tilde{\mathbf{u}}_{j,N-k}); t] \text{ and} \\ \tilde{\mathbf{u}}_i^P(t) &= \mathbf{P}_i^P[(T_N, \tilde{\mathbf{u}}_{i,N}), (T_{N-1}, \tilde{\mathbf{u}}_{i,N-1}), \dots, (T_{N-k}, \tilde{\mathbf{u}}_{i,N-k}); t] \end{aligned} \quad (76)$$

yields the predicted state variables at the macro-time point T_{N+1}

$$\hat{\mathbf{z}}_{1,N+1}^P = \hat{\mathbf{z}}_{1,N+1}(\tilde{\mathbf{u}}_j^P), \quad \hat{\mathbf{z}}_{2,N+1}^P = \hat{\mathbf{z}}_{2,N+1}(\tilde{\mathbf{u}}_i^P). \quad (77)$$

Step 2: Calculation of corrected coupling variables

- Integration of subsystem 1 and subsystem 2 from T_N to T_{N+1} with the predicted (extrapolated) coupling variables is repeated with two exceptions. The m th ($1 \leq m \leq n_{\tilde{u}_j}$) component of \mathbf{P}_j^P is replaced by the perturbed predicted (interpolation) polynomial $P_{\tilde{u}_{jm}}^{PP_m}[(T_{N+1}, \tilde{\mathbf{u}}_{jm,N+1}^P + \Delta u_m), (T_N, \tilde{\mathbf{u}}_{jm,N}), \dots, (T_{N-k+1}, \tilde{\mathbf{u}}_{jm,N-k+1}); t]$, see Fig. 7. Furthermore, the n th ($1 \leq n \leq n_{\tilde{u}_i}$) component of \mathbf{P}_i^P is replaced by the perturbed predicted (interpolation) polynomial $P_{\tilde{u}_{in}}^{PP_n}[(T_{N+1}, \tilde{\mathbf{u}}_{in,N+1}^P + \Delta u_n), (T_N, \tilde{\mathbf{u}}_{in,N}), \dots, (T_{N-k+1}, \tilde{\mathbf{u}}_{in,N-k+1}); t]$. The vectors collecting the approximation polynomials with the perturbed components m and n are denoted by $\mathbf{P}_j^{PP_m}$ and $\mathbf{P}_i^{PP_n}$. Note that Δu_m and Δu_n are user-defined increments.
- Integration of subsystem 1 and subsystem 2 from T_N to T_{N+1} with initial conditions (75a) and with the perturbed predicted coupling variables

$$\begin{aligned} \tilde{\mathbf{u}}_j^{PP_m}(t) &= \mathbf{P}_j^{PP_m}[(T_{N+1}, \tilde{\mathbf{u}}_{jm,N+1}^P + \Delta u_m), (T_N, \tilde{\mathbf{u}}_{j,N}), (T_{N-1}, \tilde{\mathbf{u}}_{j,N-1}), \dots; t] \text{ and} \\ \tilde{\mathbf{u}}_i^{PP_n}(t) &= \mathbf{P}_i^{PP_n}[(T_{N+1}, \tilde{\mathbf{u}}_{in,N+1}^P + \Delta u_n), (T_N, \tilde{\mathbf{u}}_{i,N}), (T_{N-1}, \tilde{\mathbf{u}}_{i,N-1}), \dots; t] \end{aligned} \quad (78)$$

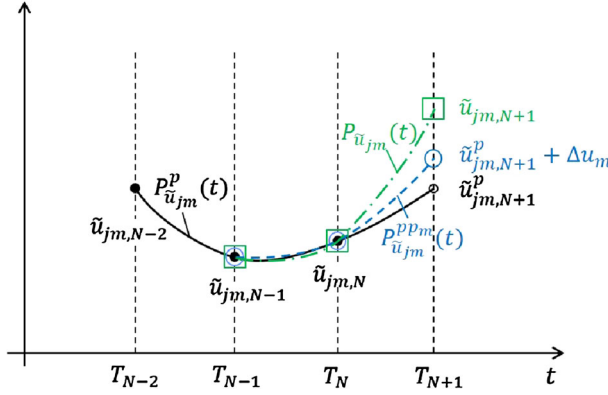


Fig. 7 Illustration of the three different approximation polynomials (polynomial degree $k = 2$) for the coupling variable $\tilde{u}_{jm}(t)$: predictor (extrapolation) polynomial $P_{\tilde{u}_{jm}}^p(t)$, perturbed predicted (interpolation) polynomial $P_{\tilde{u}_{jm}}^{ppm}(t)$, and corrector (interpolation) polynomial $P_{\tilde{u}_{jm}}^c(t)$

yields the perturbed predicted state variables at the macro-time point T_{N+1}

$$\hat{z}_{1,N+1}^{ppm} = \hat{z}_{1,N+1}(\tilde{\mathbf{u}}_j^{ppm}), \quad \hat{z}_{2,N+1}^{ppn} = \hat{z}_{2,N+1}(\tilde{\mathbf{u}}_i^{ppn}). \quad (79)$$

- With the predicted and the perturbed predicted state variables, the partial derivatives of the state vectors z_i and z_j with respect to the m th and n th coupling variable $\tilde{u}_{jm,N+1}$ and $\tilde{u}_{in,N+1}$ can be approximated by finite differences. The partial derivative of the μ th ($1 \leq \mu \leq 12$) component of z_i with respect to $\tilde{u}_{jm,N+1}$ and the partial derivative of the ν th ($1 \leq \nu \leq 12$) component of z_j with respect to $\tilde{u}_{in,N+1}$ read as

$$\begin{aligned} \frac{\partial z_{i\mu,N+1}}{\partial \tilde{u}_{jm,N+1}} \Big|_{\tilde{\mathbf{u}}_{c,N+1}^p} &\approx \frac{z_{i\mu,N+1}(\tilde{\mathbf{u}}_j^{ppm}) - z_{i\mu,N+1}(\tilde{\mathbf{u}}_j^p)}{\Delta u_m}, \\ \frac{\partial z_{j\nu,N+1}}{\partial \tilde{u}_{in,N+1}} \Big|_{\tilde{\mathbf{u}}_{c,N+1}^p} &\approx \frac{z_{j\nu,N+1}(\tilde{\mathbf{u}}_i^{ppn}) - z_{j\nu,N+1}(\tilde{\mathbf{u}}_i^p)}{\Delta u_n}. \end{aligned} \quad (80)$$

- With the help of the partial derivatives, corrected (i.e., improved) values for the coupling variables at the time point T_{N+1} can be derived. At the fixed macro-time point T_{N+1} , $\mathbf{g}_{c,N+1}$ can be considered as a function of the coupling variables $\tilde{\mathbf{u}}_{c,N+1}$

$$\mathbf{g}_{c,N+1}(\tilde{\mathbf{u}}_{c,N+1}). \quad (81)$$

Choosing $\tilde{\mathbf{u}}_{c,N+1}^p$ as expansion point and neglecting higher-order terms $\mathcal{O}(\tilde{\mathbf{u}}_{c,N+1}^2)$, a Taylor series expansion of $\mathbf{g}_{c,N+1}(\tilde{\mathbf{u}}_{c,N+1})$ with respect to $\tilde{\mathbf{u}}_{c,N+1}$ yields the linearized coupling conditions

$$\mathbf{g}_{c,N+1}^{linear}(\tilde{\mathbf{u}}_{c,N+1}) := \mathbf{g}_{c,N+1}(\tilde{\mathbf{u}}_{c,N+1}^p) + \frac{\partial \mathbf{g}_{c,N+1}}{\partial \tilde{\mathbf{u}}_{c,N+1}} \Big|_{\tilde{\mathbf{u}}_{c,N+1}^p} \cdot (\tilde{\mathbf{u}}_{c,N+1} - \tilde{\mathbf{u}}_{c,N+1}^p) = \mathbf{0}. \quad (82)$$

For the flexible fundamental joints defined in Sect. 3, the coupling conditions can be split into two parts according to

$$\begin{aligned} \mathbf{g}_{c,N+1}(\tilde{\mathbf{u}}_{c,N+1}) &= \mathbf{g}_{c,N+1}(\tilde{\mathbf{u}}_{c,N+1}, z_{c,N+1}(\tilde{\mathbf{u}}_{c,N+1})) \\ &= \tilde{\mathbf{u}}_{c,N+1} + \bar{\mathbf{g}}_{c,N+1}(z_{c,N+1}(\tilde{\mathbf{u}}_{c,N+1})). \end{aligned} \quad (83)$$

As a consequence, the Jacobian \mathbf{G} can be written as

$$\mathbf{G} = \frac{\partial \mathbf{g}_{c,N+1}}{\partial \tilde{\mathbf{u}}_{c,N+1}} \Big|_{\tilde{\mathbf{u}}_{c,N+1}^p} = \mathbf{E} + \frac{\partial \bar{\mathbf{g}}_{c,N+1}}{\partial z_{c,N+1}} \frac{\partial z_{c,N+1}}{\partial \tilde{\mathbf{u}}_{c,N+1}} \Big|_{\tilde{\mathbf{u}}_{c,N+1}^p}, \quad (84)$$

where the partial derivatives $\frac{\partial z_{c,N+1}}{\partial \tilde{\mathbf{u}}_{c,N+1}} \Big|_{\tilde{\mathbf{u}}_{c,N+1}^p}$ can approximately be calculated according to Eq. (80).

- In general, the predicted state and coupling variables do not fulfill the coupling conditions, i.e., $\mathbf{g}_{c,N+1}(\tilde{\mathbf{u}}_{c,N+1}^p) \neq \mathbf{0}$. Improved coupling variables, which fulfill the linearized coupling conditions, can be derived by solving Eq. (82) for $\tilde{\mathbf{u}}_{c,N+1}$, which yields

$$\tilde{\mathbf{u}}_{c,N+1} = \tilde{\mathbf{u}}_{c,N+1}^p - \mathbf{G}^{-1} \cdot \mathbf{g}_{c,N+1}(\tilde{\mathbf{u}}_{c,N+1}^p). \quad (85)$$

Step 3: Corrector Step

- Integration of subsystem 1 and subsystem 2 from T_N to T_{N+1} with the corrected (interpolated) coupling variables

$$\begin{aligned}\tilde{\mathbf{u}}_j(t) &= \mathbf{P}_j [(T_{N+1}, \tilde{\mathbf{u}}_{j,N+1}), (T_N, \tilde{\mathbf{u}}_{j,N}), \dots, (T_{N-k+1}, \tilde{\mathbf{u}}_{j,N-k+1}); t] \text{ and} \\ \tilde{\mathbf{u}}_i(t) &= \mathbf{P}_i [(T_{N+1}, \tilde{\mathbf{u}}_{i,N+1}), (T_N, \tilde{\mathbf{u}}_{i,N}), \dots, (T_{N-k+1}, \tilde{\mathbf{u}}_{i,N-k+1}); t]\end{aligned} \quad (86)$$

yields the corrected state variables at the macro-time point T_{N+1}

$$\hat{\mathbf{z}}_{1,N+1} = \hat{\mathbf{z}}_{1,N+1}(\tilde{\mathbf{u}}_j), \quad \hat{\mathbf{z}}_{2,N+1} = \hat{\mathbf{z}}_{2,N+1}(\tilde{\mathbf{u}}_i). \quad (87)$$

- Remark: The corrected state variables have been calculated based on the linearized coupling conditions (82). In general, however, the corrected states do not fulfill the nonlinear coupling conditions, i.e., $\mathbf{g}_{c,N+1}(\tilde{\mathbf{u}}_{c,N+1}, \mathbf{z}_{c,N+1}(\tilde{\mathbf{u}}_{c,N+1})) \neq \mathbf{0}$. To get consistent corrected coupling variables, the coupling variables may in a final evaluation step be calculated by the coupling equations and the corrected state variables, i.e., by solving

$$\mathbf{g}_{c,N+1}(\tilde{\mathbf{u}}_{c,N+1}^{\text{final}}, \mathbf{z}_{c,N+1}(\tilde{\mathbf{u}}_{c,N+1})) = \mathbf{0} \quad (88)$$

for $\tilde{\mathbf{u}}_{c,N+1}^{\text{final}}$. Choosing $\tilde{\mathbf{u}}_{c,N+1}^{\text{final}}$ from Eq. (88) instead of $\tilde{\mathbf{u}}_{c,N+1}$ from Eq. (85) as corrected coupling variables at the macro-time point T_{N+1} may improve the simulation results and the numerical stability of the approach.

4 Numerical examples

In this section, the semi-implicit co-simulation method is investigated and tested with 3 numerical examples.

4.1 Linear two-mass oscillator

As a first example, we consider the linear two-mass oscillator of Sect. 2. Simulations have been carried out with the following parameters: $m_1 = 1$, $m_2 = 2$, $c = c_1 = c_2 = c_c = 1000$ and $d = d_1 = d_2 = d_c = 10$. As initial conditions, we have chosen $x_{1,0} = x_{2,0} = 0$, $v_{1,0} = 100$, $v_{2,0} = -100$. The subsystems have been integrated with a BDF integrator (relative and absolute error tolerance $\varepsilon_{\text{rel}} = \varepsilon_{\text{abs}} = 1E-6$). In Fig. 8, the time response $x_1(t)$ of the left mass is shown for different macro-step sizes H (force/force-coupling approach, $k = 0$). Figure 9 shows the global error over the macro-step size H for the three different decomposition techniques. The curves have been generated with constant ($k = 0$), linear ($k = 1$) and quadratic ($k = 2$) approximation polynomials. As reference solution for calculating the global error, the analytical solution of Eq. (1) has been used. Please note that the dashed straight lines in Fig. 9 are auxiliary lines indicating the H^1 -, H^2 - and H^3 -lines in the log-log diagram.

The stability behavior of the explicit co-simulation approach and the semi-implicit method (force/ force-coupling) is compared in Fig. 10. The simulations have been carried out with $H = 5E-3$ for different values of c and d and for different approximation polynomials ($k = 0$, $k = 1$ and $k = 2$). Stable explicit simulations are indicated with “X” and stable semi-implicit simulations with “O”. As can be seen, the explicit scheme is unstable for larger values of c and d . The semi-implicit approach is stable in the considered parameter range for $k = 0$ and $k = 1$ and only gets unstable for $k = 2$ in the region $c > 1E4$ and $d < 5E1$. It should be mentioned that from the mechanical point of view, the two-mass oscillator is a stable system, since it is assumed that $m_1, m_2 > 0$, $c > 0$ and $d > 0$. Therefore, if a simulation shows exponentially increasing amplitudes, the instability must result from the discretization with the co-simulation approach (destabilizing effects from the subsystem integrator are not present for the considered problem).

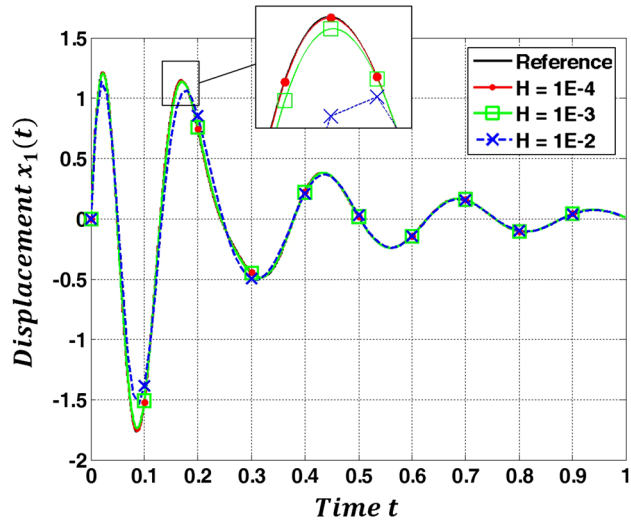


Fig. 8 Displacement $x_1(t)$ for different macro-step sizes H (force/force-coupling approach, $k = 0$)

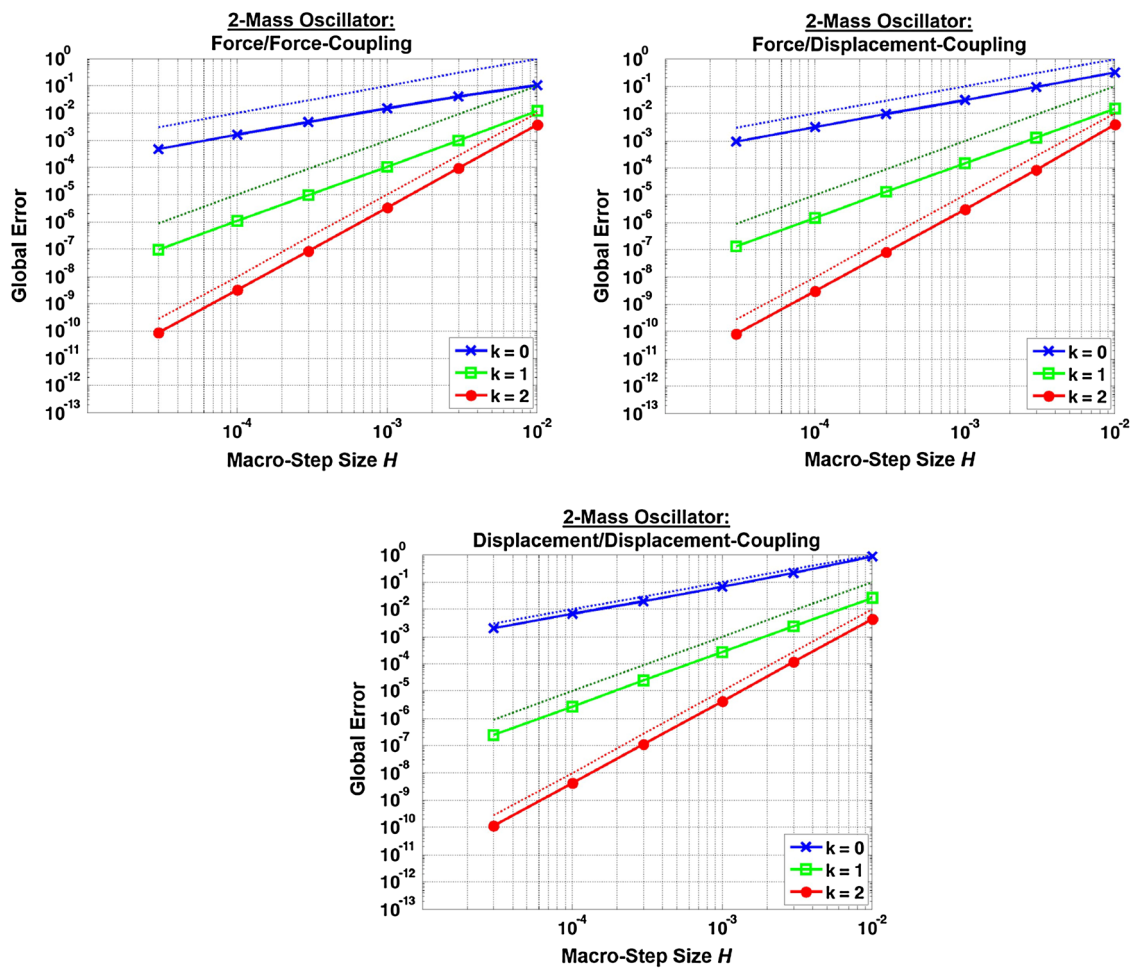


Fig. 9 Convergence plots for the linear two-mass oscillator: global error over macro-step size H . **a** Force/force-coupling approach, **b** force/displacement-coupling approach and **c** displacement/displacement-coupling approach

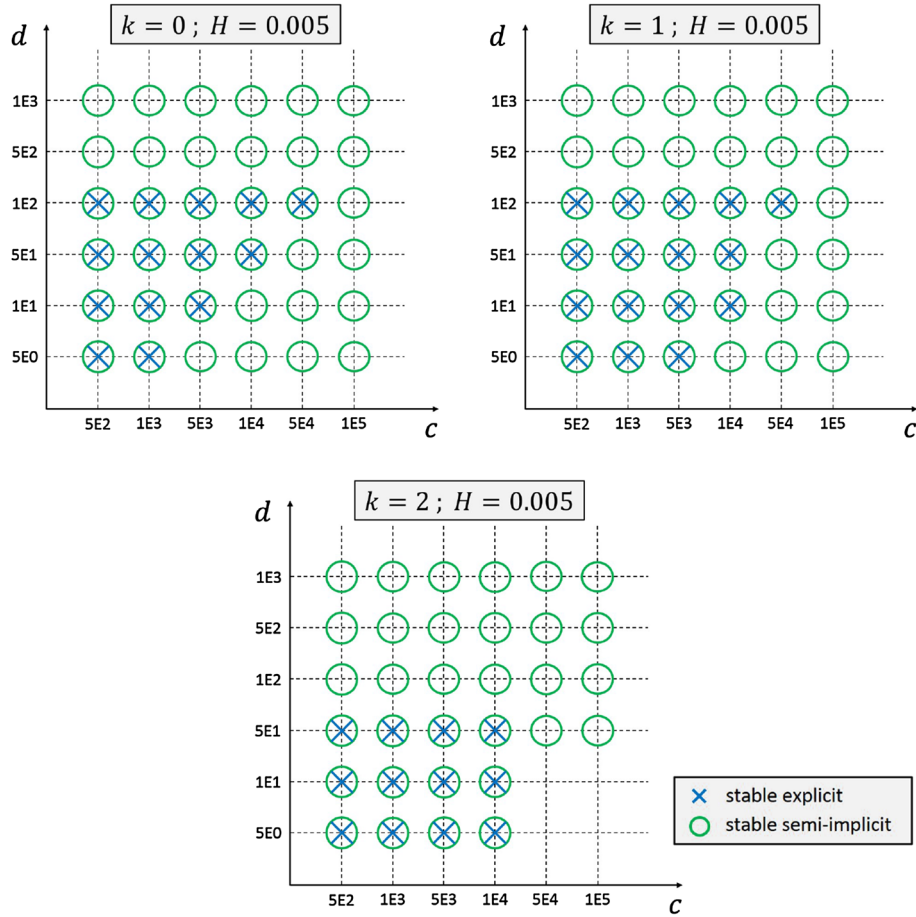


Fig. 10 Stable co-simulations of the explicit and the semi-implicit co-simulation method (force/force-coupling approach) for different stiffness coefficients c and damping coefficients d : **a** constant ($k = 0$), **b** linear ($k = 1$) and **c** quadratic ($k = 2$) approximation polynomials

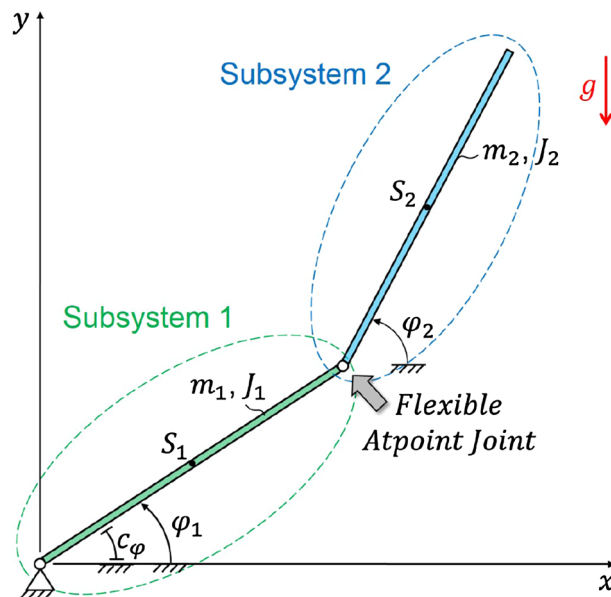


Fig. 11 Double pendulum: interpretation as two links coupled by flexible atpoint joint

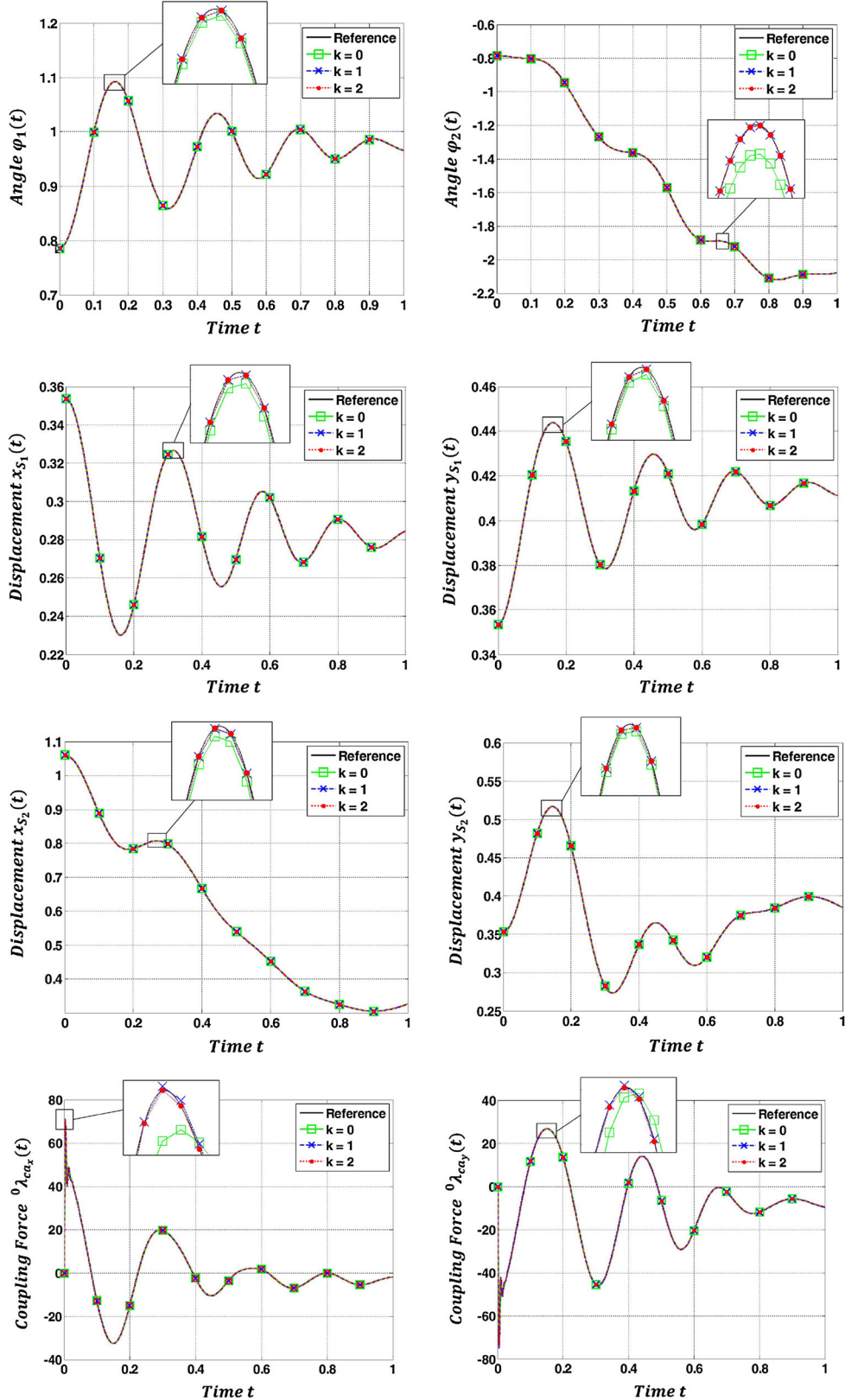


Fig. 12 Angles $\varphi_1(t)$ and $\varphi_2(t)$, displacements $x_{S_1}(t)$ and $y_{S_1}(t)$, displacements $x_{S_2}(t)$ and $y_{S_2}(t)$ as well as coupling forces ${}^0\lambda_{ca_x}(t)$ and ${}^0\lambda_{ca_y}(t)$ for $k = 0$, $k = 1$ and $k = 2$ (force/force-coupling approach, $H = 1E - 3$)

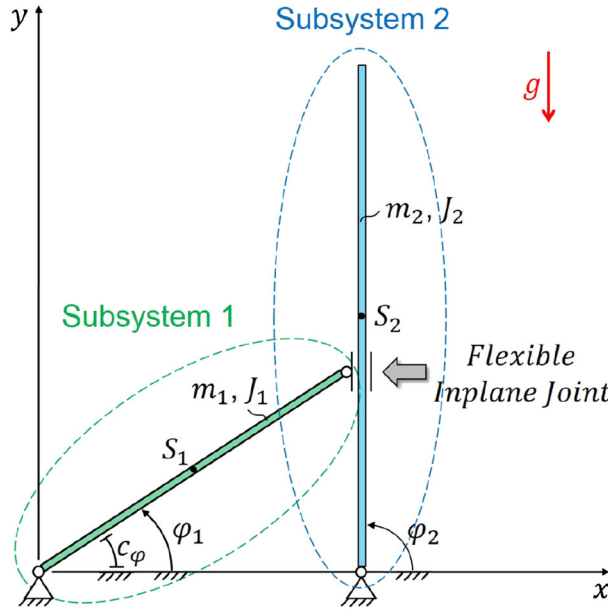


Fig. 13 Slider-crank mechanism: interpretation as two links coupled by a flexible inplane joint

4.2 Double pendulum

As a second example, we consider the planar double pendulum (masses $m_1 = m_2 = 1$, moments of inertia $J_1 = J_2 = 1/12$, lengths $l_1 = l_2 = 1$) depicted in Fig. 11. The first link is connected to ground by a rigid revolute joint and a torsional spring/damper system (spring constant $c_\varphi = 500$, damping coefficient $d_\varphi = 5$). The spring is assumed to be stress-free for $\varphi_1 = 5\pi/16$. The second link is connected to the first link by a linear flexible atpoint joint ($c_x = c_y = 1E5$, $d_x = d_y = 1E2$), which is in the planar case equivalent to a revolute joint. Gravity ($g = 9.81$) is acting in negative y -direction. As initial conditions, we have chosen $\varphi_{1,0} = \pi/4$, $\varphi_{2,0} = -\pi/4$, $\dot{\varphi}_{1,0} = \dot{\varphi}_{2,0} = 0$. The subsystems have been integrated with an implicit Runge–Kutta method (relative and absolute error tolerance $\varepsilon_{\text{rel}} = \varepsilon_{\text{abs}} = 1E - 6$). Figure 12 shows the angles $\varphi_1(t)$ and $\varphi_2(t)$, the displacements of the center of masses S_1 and S_2 in horizontal and vertical direction as well as the coupling forces ${}^0\lambda_{ca_x}(t)$ and ${}^0\lambda_{ca_y}(t)$ for $k = 0$, $k = 1$ and $k = 2$ (force/force-coupling approach, macro-step size $H = 1E - 3$). It can be seen that even for $k = 0$, the co-simulation results are close to the reference solution, which has been calculated numerically with a monolithic model. Please note that the large fluctuations in the coupling forces at the beginning of the simulation result from the stiffness of the flexible atpoint joint. Since damping is applied, oscillations due to the flexible atpoint joint are rapidly decaying.

4.3 Slider–crank mechanism

As a third example, the slider-crank mechanism is analyzed, see Fig. 13. Each subsystem consists of a rigid link, connected to ground by an ideal revolute joint. The two subsystems are coupled by a linear flexible inplane joint ($c = 1E3$, $d = 0$). Gravity ($g = 9.81$) is acting in negative y -direction. Simulations have been carried out with the following parameters: $m_1 = \sqrt{2}$, $m_2 = 2$, $J_1 = \sqrt{2}/6$, $J_2 = 2/3$, $l_1 = \sqrt{2}$, $l_2 = 2$. As initial conditions, we have chosen $\varphi_{1,0} = \pi/4$, $\varphi_{2,0} = \pi/2$, $\dot{\varphi}_{1,0} = \dot{\varphi}_{2,0} = 0$. The subsystems have been integrated with an implicit Runge–Kutta integrator (relative and absolute error tolerance $\varepsilon_{\text{rel}} = \varepsilon_{\text{abs}} = 1E - 6$). Figure 14 shows the angles $\varphi_1(t)$ and $\varphi_2(t)$, the displacements of the center of masses S_1 and S_2 in horizontal and vertical direction as well as the total energy $E_{\text{total}}(t)$ of the system (kinetic plus potential energy) for different macro-step sizes H (force/force-coupling approach, $k = 0$). The plots clearly illustrate that the co-simulation converges to the reference solution, which has been computed numerically with a monolithic model. The numerical damping due to the coupling approach is reduced for smaller macro-step sizes H .

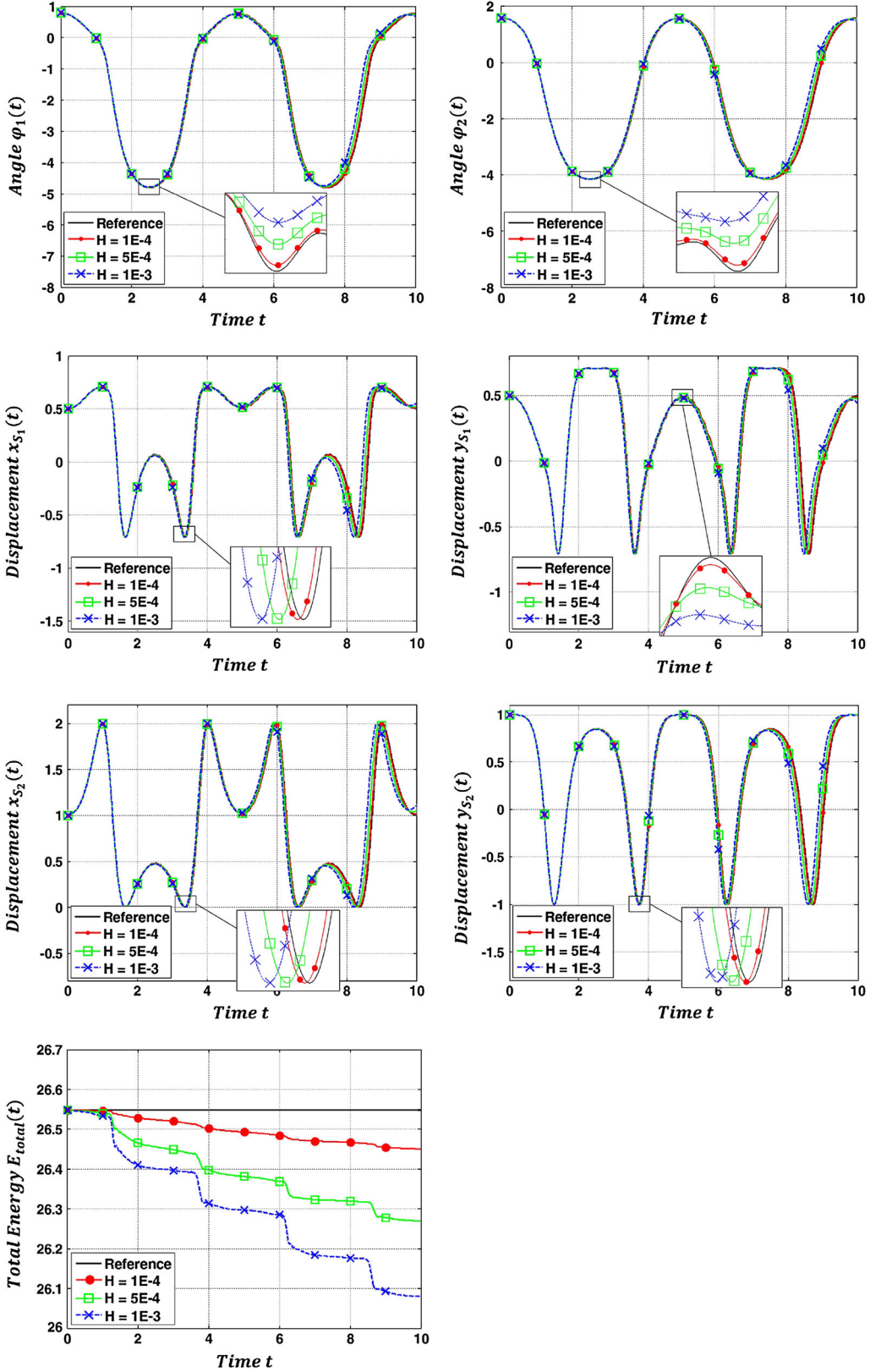


Fig. 14 Angles $\varphi_1(t)$ and $\varphi_2(t)$, displacements $x_{S1}(t)$ and $y_{S1}(t)$, displacements $x_{S2}(t)$ and $y_{S2}(t)$ as well as the total energy $E_{\text{total}}(t)$ of the system for $H = 1E - 3$, $H = 5E - 4$ and $H = 1E - 4$ (force/force-coupling approach, $k = 0$)

5 Conclusions

The presented semi-implicit co-simulation approach may provide an efficient and stable alternative to well-established coupling schemes. The numerical stability and the convergence behavior of the introduced method have been investigated with different examples. In our simulations, the semi-implicit approach has shown a better stability behavior than the explicit coupling approach. This is the main advantage of the new coupling scheme. Compared with the explicit approach, the semi-implicit method has one major drawback, namely the fact that the macro-time step has to be repeated once in order to get corrected state and coupling variables. Therefore, the subsystem solvers have to be reinitialized at the previous macro-time point T_N .

For the semi-implicit approach, a Jacobian matrix is required. In practice, the calculation of the Jacobian does not entail additional computation time, since the corresponding partial derivatives can easily be calculated in parallel with the predictor step. In contrast to implicit or semi-implicit coupling schemes, where the Jacobian matrix has the same dimension as the subsystems, the Jacobian matrix of the here introduced semi-implicit approach has very small dimensions (defined by the number of coupling conditions). The entries in the Jacobian matrix can in a straightforward manner be calculated numerically by finite differences. In the case that there exist no algebraic constraints between the coupling body i (body j) and the other bodies of subsystem 1 (subsystem 2), i.e., in the case that there are no reaction forces/torques acting on coupling body i (body j), very simple approximation formulas for the Jacobian matrix can be derived, see “Appendix A”.

It should be stressed that the accuracy and stability of the presented coupling approach may be improved by performing a complete iteration, i.e., by repeating the macro step several times with improved coupling variables until a convergence criterion is fulfilled (full-implicit co-simulation approach). Furthermore, a macro-step size controller may in a straightforward manner be implemented based on the comparison of predicted and corrected variables.

Within this paper, coupling forces ${}^0\mathbf{F}_{c_i}$ and ${}^0\mathbf{F}_{c_j}$ are expressed in the inertial reference frame K_0 and coupling torques ${}^i\mathbf{M}_{c_i}$ and ${}^j\mathbf{M}_{c_j}$ in the body-fixed systems K_{S_i} and K_{S_j} . Using commercial multibody software tools, the coupling forces can easily be implemented as space-fixed forces and the coupling torques as body-fixed torques.

Appendix A: Analytical approximation formulas for calculating the Jacobian matrix

As outlined in Sects. 2 and 3, the partial derivatives of the state variables \mathbf{z}_i , \mathbf{z}_j with respect to the coupling variables $\tilde{\mathbf{u}}_j$, $\tilde{\mathbf{u}}_i$ can in a straightforward manner be approximated by finite differences. In this Appendix, we sketch an alternative—and even more simple and efficient—way to calculate the Jacobian matrix. To demonstrate the basic idea, we focus on subsystem 1 and calculate the partial derivatives $\frac{\partial \mathbf{z}_{i,N+1}}{\partial \tilde{\mathbf{u}}_{j,N+1}} \Big|_{\tilde{\mathbf{u}}_{c,N+1}^p}$. The

basic idea is to symbolically discretize the equations of motion of the coupling body i by using an explicit integration scheme and to perform one integration step ($T_N \rightarrow T_{N+1}$). As initial conditions, the corrected state variables $\mathbf{z}_{i,N}$ at the time point T_N are used. The discretized state variables $\mathbf{z}_{i,N+1}$ are then analytically differentiated with respect to the coupling variables $\tilde{\mathbf{u}}_{j,N+1}$ so that analytical approximation formulas for the partial derivatives (Jacobian matrix) are obtained.

In the following, we assume that the reaction forces/torques are zero (${}^0\mathbf{F}_{r_i} = \mathbf{0}$, ${}^i\mathbf{M}_{r_i} = \mathbf{0}$), i.e., there exist no algebraic constraints between the coupling body i and the other bodies of subsystem 1. Hence, the equations of motion for the coupling body i are given by

Coupling body i (subsystem 1):

$$\begin{aligned} {}^0\dot{\mathbf{r}}_{S_i} &= {}^0\mathbf{v}_{S_i}, \quad {}^0\dot{\mathbf{v}}_{S_i} = \frac{1}{m_i} [{}^0\mathbf{F}_{a_i}(\hat{\mathbf{z}}_1, t) + {}^0\mathbf{F}_{c_i}(\mathbf{z}_i, \tilde{\mathbf{u}}_j)], \\ \dot{\gamma}_i &= \mathbf{B}(\gamma_i) {}^i\omega_i, \quad {}^i\dot{\omega}_i = {}^i\mathbf{J}_i^{-1} [-{}^i\omega_i \times {}^i\mathbf{J}_i {}^i\omega_i + {}^i\mathbf{M}_{a_i}(\hat{\mathbf{z}}_1, t) + {}^i\mathbf{M}_{c_i}(\mathbf{z}_i, \tilde{\mathbf{u}}_j)]. \end{aligned} \quad (89)$$

We now suppose that the state and the coupling variables ${}^0\mathbf{r}_{S_i,N}$, ${}^0\mathbf{v}_{S_i,N}$, $\gamma_{i,N}$, ${}^i\omega_{i,N}$, $\tilde{\mathbf{u}}_{j,N}$ are known at the macro-time point T_N . Furthermore, we assume that constant polynomials are used for approximating the coupling variables (polynomial degree $k = 0$), i.e., $\tilde{\mathbf{u}}_j^p(t) = \tilde{\mathbf{u}}_{j,N+1}^p = \tilde{\mathbf{u}}_{j,N} = \text{const}$. Discretizing Eq. (89) by using Heun’s method (explicit second-order Runge–Kutta method), performing one integration step from T_N to $T_{N+1} = T_N + H$ and calculating the partial derivatives with respect to $\tilde{\mathbf{u}}_{j,N+1}$ yields the subsequent approximations

Coupling body i (subsystem 1):

$$\begin{aligned}
 \frac{\partial {}^0\mathbf{r}_{S_i,N+1}}{\partial \tilde{\mathbf{u}}_{j,N+1}} \Big|_{\tilde{\mathbf{u}}_{j,N+1}^p} &\approx \frac{H^2}{2m_i} \frac{\partial {}^0\mathbf{F}_{c_i}(\mathbf{z}_{i,N}, \tilde{\mathbf{u}}_{j,N+1})}{\partial \tilde{\mathbf{u}}_{j,N+1}} \Big|_{\tilde{\mathbf{u}}_{j,N+1}^p}, \\
 \frac{\partial {}^0\mathbf{v}_{S_i,N+1}}{\partial \tilde{\mathbf{u}}_{j,N+1}} \Big|_{\tilde{\mathbf{u}}_{j,N+1}^p} &\approx \frac{H}{m_i} \frac{\partial {}^0\mathbf{F}_{c_i}(\mathbf{z}_{i,N}, \tilde{\mathbf{u}}_{j,N+1})}{\partial \tilde{\mathbf{u}}_{j,N+1}} \Big|_{\tilde{\mathbf{u}}_{j,N+1}^p}, \quad (*) \\
 \frac{\partial \boldsymbol{\gamma}_{i,N+1}}{\partial \tilde{\mathbf{u}}_{j,N+1}} \Big|_{\tilde{\mathbf{u}}_{j,N+1}^p} &\approx \frac{H^2}{2} \mathbf{B}(\boldsymbol{\gamma}_{i,N})^i \mathbf{J}_i^{-1} \frac{\partial {}^i\mathbf{M}_{c_i}(\mathbf{z}_{i,N}, \tilde{\mathbf{u}}_{j,N+1})}{\partial \tilde{\mathbf{u}}_{j,N+1}} \Big|_{\tilde{\mathbf{u}}_{j,N+1}^p}, \\
 \frac{\partial {}^i\boldsymbol{\omega}_{i,N+1}}{\partial \tilde{\mathbf{u}}_{j,N+1}} \Big|_{\tilde{\mathbf{u}}_{j,N+1}^p} &\approx H^i \mathbf{J}_i^{-1} \frac{\partial {}^i\mathbf{M}_{c_i}(\mathbf{z}_{i,N}, \tilde{\mathbf{u}}_{j,N+1})}{\partial \tilde{\mathbf{u}}_{j,N+1}} \Big|_{\tilde{\mathbf{u}}_{j,N+1}^p}. \quad (**)
 \end{aligned} \tag{90}$$

It should be stressed that a second-order integration scheme is required to calculate the partial derivatives $\frac{\partial {}^0\mathbf{r}_{S_i,N+1}}{\partial \tilde{\mathbf{u}}_{j,N+1}}$ and $\frac{\partial \boldsymbol{\gamma}_{i,N+1}}{\partial \tilde{\mathbf{u}}_{j,N+1}}$, since the corresponding kinematical differential equations do not explicitly contain the coupling variables. For calculating the partial derivatives $\frac{\partial {}^0\mathbf{v}_{S_i,N+1}}{\partial \tilde{\mathbf{u}}_{j,N+1}}$ and $\frac{\partial {}^i\boldsymbol{\omega}_{i,N+1}}{\partial \tilde{\mathbf{u}}_{j,N+1}}$, a first-order integration scheme would be sufficient. Integration with Euler explicit directly yields the approximations (*) and (**) in Eq. (90).

If higher-order polynomials are used to approximate the coupling variables ($k \geq 1$), discretization with second-order methods is not sufficient and higher-order integration schemes have to be applied. In the case of linear approximation polynomials ($k = 1$), a third-order Runge–Kutta method would be necessary, for instance.

Remark: Improved approximation formulas for the partial derivatives can in a straightforward manner be derived with the help of the matrix exponential function. Therefore, the equations of motion of the subsystem are linearized with respect to the subsystem states and with respect to the time, which yields a system of linear time-invariant differential equations. The solution of the linearized system can be expanded in a Taylor series with respect to time by means of the matrix exponential function. Analytical differentiation of the truncated series solution with respect to the coupling variables yields improved analytical approximation formulas. Using only the first series term gives the approximation formulas of Eq. (90).

If the reaction forces/torques are not zero (${}^0\mathbf{F}_{r_i} \neq \mathbf{0}$ or ${}^i\mathbf{M}_{r_i} \neq \mathbf{0}$), i.e., subsystem one is described by a DAE system, direct application of explicit integration schemes to calculate the Jacobian matrix is not possible. One simple way to treat that case is to derive the underlying ODE of the DAE system and to proceed as described above. The numerical drift effect, which occurs during the numerical integration of the underlying ODE, is not problematic here, since only one integration step is performed and because the initial conditions are updated by the corrected state variables after each step. A second way is the application of implicit integration schemes.

Example 1: We consider the 2-mass oscillator of Sect. 2 and apply a force/force-coupling approach (polynomial degree $k = 0$). Then, Eq. (90) yields the following partial derivatives

$$\begin{aligned}
 \frac{\partial x_{1,N+1}}{\partial \lambda_{c,N+1}} \Big|_{\lambda_{c,N+1}^p} &\approx \frac{H^2}{2m_1}, \quad \frac{\partial v_{1,N+1}}{\partial \lambda_{c,N+1}} \Big|_{\lambda_{c,N+1}^p} \approx \frac{H}{m_1}, \\
 \frac{\partial x_{2,N+1}}{\partial \lambda_{c,N+1}} \Big|_{\lambda_{c,N+1}^p} &\approx -\frac{H^2}{2m_2}, \quad \frac{\partial v_{2,N+1}}{\partial \lambda_{c,N+1}} \Big|_{\lambda_{c,N+1}^p} \approx -\frac{H}{m_2}.
 \end{aligned} \tag{91}$$

Example 2: The two subsystems of the slider-crank mechanism of Sect. 4.3 are mathematically described by DAE systems. Based on the corresponding underlying ODE system, Eq. (90) yields the following partial derivatives for subsystem 1 (force/force-coupling approach, $k = 0$)

$$\frac{\partial x_{S_1,N+1}}{\partial \lambda_{cd,N+1}} \Big|_{\lambda_{cd,N+1}^p} \approx -\frac{3H^2}{4m_1} \sin \tilde{\varphi}_{2,N+1}^p \sin^2 \varphi_{1,N} - \frac{3H^2}{4m_1} \sin \varphi_{1,N} \cos \varphi_{1,N} \cos \tilde{\varphi}_{2,N+1}^p,$$

$$\begin{aligned}
\frac{\partial y_{S1,N+1}}{\partial \lambda_{cd,N+1}} \Big|_{\lambda_{cd,N+1}^p} &\approx \frac{3H^2}{4m_1} \cos \tilde{\varphi}_{2,N+1}^p \cos^2 \varphi_{1,N} + \frac{3H^2}{4m_1} \sin \tilde{\varphi}_{2,N+1}^p \sin \varphi_{1,N} \cos \varphi_{1,N}, \\
\frac{\partial v_{Sx1,N+1}}{\partial \lambda_{cd,N+1}} \Big|_{\lambda_{cd,N+1}^p} &\approx -\frac{3H}{2m_1} \sin \tilde{\varphi}_{2,N+1}^p \sin^2 \varphi_{1,N} - \frac{3H}{2m_1} \sin \varphi_{1,N} \cos \varphi_{1,N} \cos \tilde{\varphi}_{2,N+1}^p, \\
\frac{\partial v_{Sy1,N+1}}{\partial \lambda_{cd,N+1}} \Big|_{\lambda_{cd,N+1}^p} &\approx \frac{3H}{2m_1} \cos \tilde{\varphi}_{2,N+1}^p \cos^2 \varphi_{1,N} + \frac{3H}{2m_1} \sin \tilde{\varphi}_{2,N+1}^p \sin \varphi_{1,N} \cos \varphi_{1,N}, \\
\frac{\partial \varphi_{1,N+1}}{\partial \lambda_{cd,N+1}} \Big|_{\lambda_{cd,N+1}^p} &\approx \frac{H^2 l_1}{8J_1} (\cos \varphi_{1,N} \cos \tilde{\varphi}_{2,N+1}^p + \sin \varphi_{1,N} \sin \tilde{\varphi}_{2,N+1}^p), \\
\frac{\partial \omega_{1,N+1}}{\partial \lambda_{cd,N+1}} \Big|_{\lambda_{cd,N+1}^p} &\approx \frac{H l_1}{4J_1} (\cos \varphi_{1,N} \cos \tilde{\varphi}_{2,N+1}^p + \sin \varphi_{1,N} \sin \tilde{\varphi}_{2,N+1}^p), \\
\frac{\partial x_{S1,N+1}}{\partial \tilde{\varphi}_{2,N+1}} \Big|_{\tilde{\varphi}_{2,N+1}^p} &\approx \frac{3\lambda_{cd,N+1}^p H^2}{4m_1} (\cos \tilde{\varphi}_{2,N+1}^p \sin^2 \varphi_{1,N} + \cos \varphi_{1,N} \sin \varphi_{1,N} \sin \tilde{\varphi}_{2,N+1}^p), \\
\frac{\partial y_{S1,N+1}}{\partial \tilde{\varphi}_{2,N+1}} \Big|_{\tilde{\varphi}_{2,N+1}^p} &\approx \frac{3\lambda_{cd,N+1}^p H^2}{4m_1} (\cos \tilde{\varphi}_{2,N+1}^p \sin \varphi_{1,N} \cos \varphi_{1,N} - \sin \tilde{\varphi}_{2,N+1}^p \cos^2 \varphi_{1,N}), \\
\frac{\partial v_{Sx1,N+1}}{\partial \tilde{\varphi}_{2,N+1}} \Big|_{\tilde{\varphi}_{2,N+1}^p} &\approx \frac{3\lambda_{cd,N+1}^p H}{2m_1} (\cos \tilde{\varphi}_{2,N+1}^p \sin^2 \varphi_{1,N} + \cos \varphi_{1,N} \sin \varphi_{1,N} \sin \tilde{\varphi}_{2,N+1}^p), \\
\frac{\partial v_{Sy1,N+1}}{\partial \tilde{\varphi}_{2,N+1}} \Big|_{\tilde{\varphi}_{2,N+1}^p} &\approx \frac{3\lambda_{cd,N+1}^p H}{2m_1} (\cos \tilde{\varphi}_{2,N+1}^p \sin \varphi_{1,N} \cos \varphi_{1,N} - \sin \tilde{\varphi}_{2,N+1}^p \cos^2 \varphi_{1,N}), \\
\frac{\partial \varphi_{1,N+1}}{\partial \tilde{\varphi}_{2,N+1}} \Big|_{\tilde{\varphi}_{2,N+1}^p} &\approx \frac{\lambda_{cd,N+1}^p l_1 H^2}{8J_1} (\sin \varphi_{1,N} \cos \tilde{\varphi}_{2,N+1}^p - \cos \varphi_{1,N} \sin \tilde{\varphi}_{2,N+1}^p), \\
\frac{\partial \omega_{1,N+1}}{\partial \tilde{\varphi}_{2,N+1}} \Big|_{\tilde{\varphi}_{2,N+1}^p} &\approx \frac{\lambda_{cd,N+1}^p l_1 H}{4J_1} (\sin \varphi_{1,N} \cos \tilde{\varphi}_{2,N+1}^p - \cos \varphi_{1,N} \sin \tilde{\varphi}_{2,N+1}^p). \tag{92}
\end{aligned}$$

Appendix B: Proof of zero-stability

The semi-implicit coupling approach presented in this paper is zero-stable. The proof is sketched in the following for the case that constant approximation polynomials are used ($k = 0$). We assume that both subsystems are integrated with zero-stable subsystem integrators, i.e., we ride on the assumption that the subsystem state variables and especially the state variables of the coupling bodies converge. Hence,

$$z_{c,N+1} = z_{c,N} = \dots = z_{c,0} \tag{93}$$

is fulfilled for $H \rightarrow 0$. To proof the zero-stability of the semi-implicit co-simulation approach, it therefore remains to show that the coupling variables also converge, i.e., to proof that $\tilde{u}_{c,N+1} = \tilde{u}_{c,N} = \dots = \tilde{u}_{c,0}$ for $H \rightarrow 0$. As a consequence of Eq. (93), the first term in Eq. (82) vanishes for infinitesimal step sizes, i.e.,

$$\mathbf{g}_{c,N+1}(\tilde{u}_{c,N+1}^p) \rightarrow \mathbf{0} \text{ for } H \rightarrow 0. \tag{94}$$

Regarding the flexible joints defined in Sect. 3, the coupling conditions $\mathbf{g}_{c,N+1}$ can be split into two parts

$$\mathbf{g}_{c,N+1}(\tilde{u}_{c,N+1}, z_{c,N+1}(\tilde{u}_{c,N+1})) = \tilde{u}_{c,N+1} + \bar{\mathbf{g}}_{c,N+1}(z_{c,N+1}(\tilde{u}_{c,N+1})). \tag{95}$$

Therefore, the Jacobian can also be subdivided into two parts according to

$$\mathbf{G} = \frac{\partial \mathbf{g}_{c,N+1}}{\partial \tilde{u}_{c,N+1}} \Big|_{\tilde{u}_{c,N+1}^p} = \mathbf{E} + \frac{\partial \bar{\mathbf{g}}_{c,N+1}}{\partial \tilde{u}_{c,N+1}} \Big|_{\tilde{u}_{c,N+1}^p}. \tag{96}$$

The second term $\frac{\partial \bar{g}_{c,N+1}}{\partial \tilde{u}_{c,N+1}} \Big|_{\tilde{u}_{c,N+1}^p}$ in the above equation vanishes for $H \rightarrow 0$. Therefore, we get

$$\mathbf{G} = \mathbf{E} \text{ for } H \rightarrow 0. \quad (97)$$

Inserting (94) and (97) in Eq. (82) yields

$$\underbrace{\mathbf{g}_{c,N+1}(\tilde{u}_{c,N+1}^p)}_{=0 \text{ for } H \rightarrow 0} + (\mathbf{E} + \underbrace{\frac{\partial \bar{g}_{c,N+1}}{\partial \tilde{u}_{c,N+1}} \Big|_{\tilde{u}_{c,N+1}^p}}_{=0 \text{ for } H \rightarrow 0}) \cdot (\tilde{u}_{c,N+1} - \tilde{u}_{c,N+1}^p) = \mathbf{0} \\ \implies \tilde{u}_{c,N+1} = \tilde{u}_{c,N+1}^p \text{ for } H \rightarrow 0.$$
(98)

Since $\tilde{u}_{c,N+1}^p = \tilde{u}_{c,N}$ for the case of constant approximation, one can conclude that $\tilde{u}_{c,N+1} = \tilde{u}_{c,N}$ and finally that $\tilde{u}_{c,N+1} = \tilde{u}_{c,N} = \dots = \tilde{u}_{c,0} = \mathbf{0}$.

Appendix C: Alternative coupling formulation for flexible perpendicular joint with force/force-coupling

The formulations for connecting the coupling bodies i and j with flexible joints presented in Sect. 3 may be replaced by alternative formulations. To show this, we present an alternative implementation of the flexible perpendicular joint in connection with a force/force-coupling approach, see Eq. (68). Instead of calculating the scalar-valued coupling torque λ_{cp} by the scalar coupling condition g_{cp} , Eq. (68) may be replaced by the following formulation

$$\begin{aligned} {}^0\mathbf{F}_{ci} &= \mathbf{0}, & {}^i\mathbf{M}_{ci} &= {}^{i0}\mathbf{T}(\boldsymbol{\gamma}_i) {}^0\lambda_{cp}, \\ {}^0\mathbf{F}_{cj} &= \mathbf{0}, & {}^j\mathbf{M}_{cj} &= {}^{j0}\mathbf{T}(\boldsymbol{\gamma}_j) {}^0\lambda_{cp}, \\ \mathbf{g}_{cp} &:= {}^0\lambda_{cp} - {}^{0i}\mathbf{T}(\boldsymbol{\gamma}_i) {}^i\mathbf{e}_i \times {}^{0j}\mathbf{T}(\boldsymbol{\gamma}_j) {}^j\mathbf{e}_j f_{cp}(\boldsymbol{\gamma}_i, {}^i\boldsymbol{\omega}_i, \boldsymbol{\gamma}_j, {}^j\boldsymbol{\omega}_j) = \mathbf{0} \end{aligned} \quad (99)$$

with ${}^0\lambda_{cp} = ({}^0\lambda_{cp_x} {}^0\lambda_{cp_y} {}^0\lambda_{cp_z})^T$. An advantage of this formulation is that the number of coupling conditions is reduced.

Appendix D: Simplified coupling formulation for flexible perpendicular joint with force/force-coupling

Applying, for instance, a flexible perpendicular joint in connection with a force/force-coupling approach, the coupling variables $\tilde{\boldsymbol{\gamma}}_j$ and $\tilde{\boldsymbol{\gamma}}_i$ have to be defined in order to calculate the coupling torques ${}^i\mathbf{M}_{ci}$ and ${}^j\mathbf{M}_{cj}$, see Sect. 3.3.3. In the following, we assume that the coupling stiffness is high so that the vectors \mathbf{e}_i and \mathbf{e}_j almost remain perpendicular. Considering subsystem 1, λ_{cp} then reflects the magnitude and ${}^i\mathbf{e}_i \times {}^{ij}\mathbf{T}(\boldsymbol{\gamma}_i, \tilde{\boldsymbol{\gamma}}_j) {}^j\mathbf{e}_j$ the direction of ${}^i\mathbf{M}_{ci}$. The idea of the simplified formulation is to modify the expression for the direction of the torque by replacing $\tilde{\boldsymbol{\gamma}}_j$ with the constant value $\boldsymbol{\gamma}_{j,N}$ within the macro-time step $T_N \rightarrow T_{N+1}$. Then, the simplified coupling forces/torques and the coupling condition read as

$$\begin{aligned} {}^0\mathbf{F}_{ci} &= \mathbf{0}, & {}^i\mathbf{M}_{ci} &= {}^i\mathbf{e}_i \times {}^{ij}\mathbf{T}(\boldsymbol{\gamma}_i, \boldsymbol{\gamma}_{j,N}) {}^j\mathbf{e}_j \lambda_{cp}, \\ {}^0\mathbf{F}_{cj} &= \mathbf{0}, & {}^j\mathbf{M}_{cj} &= {}^j\mathbf{e}_j \times {}^{ji}\mathbf{T}(\boldsymbol{\gamma}_{i,N}, \boldsymbol{\gamma}_j) {}^i\mathbf{e}_i \lambda_{cp}, \\ g_{cp} &:= \lambda_{cp} - f_{cp}(\boldsymbol{\gamma}_i, {}^i\boldsymbol{\omega}_i, \boldsymbol{\gamma}_j, {}^j\boldsymbol{\omega}_j) = 0. \end{aligned} \quad (100)$$

The advantage of the simplified formulation is the fact that the coupling conditions $\mathbf{g}_{c\gamma_i}$ and $\mathbf{g}_{c\gamma_j}$ are neglected. Equivalent simplified formulations can be derived for other flexible joints.

References

1. Busch, M.: Zur effizienten Kopplung von Simulationsprogrammen (On the efficient coupling of simulation codes). PhD Thesis, University of Kassel, Germany, Kassel University Press, (2012), ISBN-13: 978-3862192960
2. Busch, M., Schweizer, B.: Coupled simulation of multibody and finite element systems: an efficient and robust semi-implicit coupling approach. *Arch. Appl. Mech.* **82**(6), 723–741 (2012)
3. Busch, M., Schweizer, B.: Numerical stability and accuracy of different co-simulation techniques: analytical investigations based on a 2-DOF test model. In: Proceedings of the 1st Joint International Conference on Multibody System Dynamics, Lappeenranta, (2010)
4. Carstens, V., Kemme, R., Schmitt, S.: Coupled simulation of flow-structure interaction in turbomachinery. *Aerosp. Sci. Technol.* **7**, 298–306 (2003)
5. Dörfel, M.R., Simeon, B.: Analysis and acceleration of a fluid-structure interaction coupling scheme. *Numer. Math. Adv. Appl.*, 307–315 (2010)
6. Eberhard, P., Gausele, T., Heisel, U., Storchak, M.: A discrete element material model used in a co-simulated charpy impact test and for heat transfer. In: Proceedings 1st International Conference on Process Machine Interactions, Hannover, 3–4 Sept 2008
7. Friedrich, M., Ulrich, H.: A parallel co-simulation for mechatronic systems. In: Proceedings of the 1st Joint International Conference on Multibody System Dynamics, Lappeenranta (2010)
8. Gonzalez, F., Gonzalez, M., Cuadrado, J.: Weak coupling of multibody dynamics and block diagram simulation tools. In: Proceedings of IDETC/CIE 2009, San Diego, USA, Aug. 30 Sept. 2 (2009)
9. Gu, B., Asada, H.H.: Co-simulation of algebraically coupled dynamic subsystems without disclosure of proprietary subsystem models. *J. Dyn. Syst. Meas. Control* **126**, 1–13 (2004). doi:[10.1115/1.1648307](https://doi.org/10.1115/1.1648307)
10. Haug, E.J.: Computer-Aided Kinematics and Dynamics of Mechanical Systems. Allyn and Bacon, Boston (1989)
11. Helduser, S., Stuewing, M., Liebig, S., Dronka, S.: Development of electro-hydraulic actuators using linked simulation and hardware-in-the-loop technology. In: Burrows, C., Edge, K. (eds.) Power Transmission and Motion Control 2001, Professional Engineering Publishing, Bath, UK, pp. 49–56 (2001)
12. Hippmann, G., Arnold, M., Schittenhelm, M.: Efficient simulation of bush and roller chain drives. In: Goicoeal, J., Cuadrado, J., Orden, J.G. (eds.) Proceedings of ECCOMAS Thematic Conference on Advances in Computational Multibody Dynamics, Madrid, pp. 1–18 (2005)
13. Kübler, R., Schiehlen, W.: Two methods of simulator coupling. *Mathematical and Computer Modelling of Dynamical Systems* **6**, 93–113 (2000)
14. Lehnart, A., Fleissner, F., Eberhard, P.: Using SPH in a co-simulation approach to simulate sloshing in tank vehicles. In: Proceedings SPHERIC4, Nantes, France, 27.-29.5 (2009)
15. Meynen, S., Mayer, J., Schäfer, M.: Coupling algorithms for the numerical simulation of fluid-structure-interaction problems. *ECCOMAS 2000: European Congress on Computational Methods in Applied Sciences and Engineering*, Barcelona (2000)
16. Schäfer, M., Yigit, S., Heck, M.: Implicit partitioned fluid-structure interaction coupling. *ASME, PVP2006-ICPVT11-93184*, Vancouver, Canada (2006)
17. Schweizer, B., Lu, D.: Predictor/corrector co-simulation approaches for solver coupling with algebraic constraints. *ZAMM-J. Appl. Math. Mech.* (2014). doi:[10.1002/zamm.201300191](https://doi.org/10.1002/zamm.201300191)
18. Schweizer, B., Lu, D.: Co-simulation methods for solver coupling with algebraic constraints: semi-implicit coupling techniques. In: Proceedings of The 3rd Joint International Conference on Multibody System Dynamics and The 7th Asian Conference on Multibody Dynamics, IMSD 2014, ACMD 2014, Bexco, Busan, Korea, June 30–July 3 (2014)
19. Schweizer, B., Lu, D.: Stabilized index-2 co-simulation approach for solver coupling with algebraic constraints. *Multibody Syst. Dyn.* (2014). doi:[10.1007/s11044-014-9422-y](https://doi.org/10.1007/s11044-014-9422-y)
20. Vaculin, O., Krueger, W.R., Valasek, M.: Overview of coupling of multibody and control engineering tools. *Veh. Syst. Dyn.* **41**, 415–429 (2004)
21. Woernle, C.: Mehrkörpersysteme (Multibody systems). Springer, Berlin (2011)
22. Wuensche, S., Clauß, C., Schwarz, P., Winkler, F.: Electro-thermal circuit simulation using simulator coupling. *IEEE Trans. Very Large Scale Integr. (VLSI) Syst.* **5**, 277–282 (1997)